

FINAL TECHNICAL REPORT
Award Number: G14AP00049

Title: “Improving Regional Ground Motion Attenuation Boundaries and Models in the CEUS and Developing a Gulf Coast Empirical GMPE Using EarthScope USArray Data for Use in the National Seismic Hazards Mapping Project”

Chris H. Cramer and Md. Nayeem Al Noman
Center for Earthquake Research and Information
University of Memphis
3890 Central Ave
Memphis, TN 38152-3050
901-678-4992
FAX: 901-678-4734
cramer@ceri.memphis.edu

June 1, 2014 – May 31, 2016

Submitted: August 17, 2016

“Research supported by the U.S. Geological Survey (USGS), Department of Interior, under USGS award number G14AP00049. The views and conclusions contained in this document are those of the authors and should not be interpreted as necessarily representing the official policies, either expressed or implied, of the U.S. Government.”

Abstract

EarthScope USArray provides an excellent opportunity to improve the scientific understanding of crustal attenuation in the continental US. Previously we were funded to study major Q boundaries, regional attenuation, and develop mid-continent ENA empirical ground motion prediction equations (GMPEs) (USGS grants G12AP20016 and GP13AP00030) using data from the USArray and the Next Generation Attenuation (NGA) East ground motion database. We conducted an initial 2-year phase in 2012-2013 focused on defining Q boundaries among western US (WUS), central and eastern US (CEUS), and the Gulf Coast regions west of the Mississippi River and better defining regional Q within these major regions. The “Q” here is apparent Q due to the decay of ground motion with distance and not material Q. We developed mid-continent ENA empirical GMPEs as part of the NGA East effort (Al Noman et al., 2012, Al Noman, 2013, Al Noman and Cramer, 2015). We found the WUS/CEUS Q boundary to be farther west of 100°W and following the eastern range front of the Rocky Mountains. The Q boundaries all seem to be fairly sharp features with transitions less than the 70 km spacing of the USArray.

Under this two-year grant (G14AP00049) we defined (1) the location and character of Q transitions between major tectonic regions, particularly in the Gulf Coast region, using transects of USArray (TA) observations across these transitions to look for major changes in regional Q, (2) the regional Q within our defined Gulf Coast region and, as a separate region, Florida using the results from (1) and the approach of Benz et al. (1997) and Erickson et al (2004), and (3) an empirical GMPE for the Gulf Coast region using the NGA east database, USArray data from (1), and close-in records (less than 60 km in rupture distance) from the 2010 M7.1 Darfield, New Zealand earthquake. We detected the CEUS/Gulf Coast transition in Texas, Oklahoma, Arkansas, Mississippi, Alabama, Georgia, and the Florida panhandle, demonstrating the ability to find this transition from the limited earthquake observations available. The location of the CEUS/Gulf Coast boundary is different from the proposed boundary location in the EPRI (1993) and NGA East (Dreiling et al, 2014) regionalization studies, which are based on few direct Q observations. The observed boundary location is roughly coincident with the Thomas (2010) Alabama-Oklahoma transform and the Oacheta thrust, except it extends more into central Oklahoma because of other rift structures. Regional $Q(f) = Q_0 * f^\eta$ estimated within our Gulf Coast boundary is $Q_0 = 259 +24/-22$ and $\eta = 0.715 \pm 0.013$ over a broad frequency band of 0.1 to 16 Hz. Q for Florida, except the panhandle, seems to be constant near 1000. For the Appalachians and Atlantic Coastal Plain, $Q(f)$ is similar to mid-continent Q as shown by previous studies. We also relate our differing regional Q values to intensity observations in Oklahoma by Hough and Page (2015) and discuss intensity decay with distance affected by regional Q as used in comparisons of potential induced versus natural earthquake intensity based magnitudes as they relate to source parameters like stress drop.

Approach

We started with selecting the events that have good USArray (TA) station coverage in the possible boundary locations between the major tectonic regions of continental CEUS and Gulf Coast. The emphasis initially is on larger magnitude earthquakes to have good signal to noise over the large distances from the event covered by USArray. Then we used smaller magnitude events to provide targeted transects to help fill in the details of the attenuation transition boundaries.

Data processing included data retrieval, instrument correction, and band-pass filtering to a range of frequencies with acceptable signal-to-noise (greater than one). The procedures employed are the same as used in developing the Next Generation Attenuation (NGA) East database of ground motions (Cramer, 2008, and Cramer et al., 2009, 2011). A part of this effort is quality assurance to remove records with data problems and insufficient bandwidth in the 0.1 to 20 Hz range.

Additionally, we estimated Brune stress drop (stress parameter) from corner frequency estimates made from the tangential component of the velocity Fourier spectrum using close-in recordings generally less than 50 km from the epicenter. For velocity spectra the Brune corner frequency forms the peak of the spectrum. Because Brune stress drop is for body waves, care has been taken to avoid contaminating spectral peaks from surface waves, nearby-building interactions, and soil resonances by examining the time-series records, vertical component velocity spectra, and pre-event noise spectra as needed.

We then processed the data for peak ground acceleration and velocity, and for spectral acceleration at 0.2 sec and 1.0 sec and plotted the profile of those ground motions against epicentral distance. We looked beyond 150 km for any strong change in the slope that is obvious in the ground motion profile. Vertical component amplitudes, mainly at 0.2 and 1.0 s, were used to reduce noise due to the effects of site geology on horizontal components. The location of the change in slope gives us a possible estimate of the transition boundary between the tectonic regions. In some cases, due to sparse station coverage, locating the transition in the slope precisely is difficult within the 70 km spacing of the TA. However, these transects help constrain the location of the boundary.

To assist with the identification of the Q transition boundary we fit a decay with distance trend for a reference profile entirely within the CEUS mid-continent Q region. We fit observations of amplitudes with distance at a specific frequency to the form

$$\ln(y) = A + C \cdot \text{dist} - 0.5 \cdot \ln(\text{dist}), \quad (1)$$

where y is maximum amplitude at frequency f , dist is epicentral distance, and A and C are constants. \ln is natural logarithm. Geometrical spreading is assumed to be $R^{-0.5}$, which is typical at distances beyond 150 to 200 km in ENA (Atkinson and Mereu, 1992). The resulting reference profile decay with distance and its 95% confidence limit were then compared with the decay with distance trend for a profile crossing the expected location of the Q transition boundary and any strong deviation from the reference trend used to identify the location of the boundary.

An example of this decay with distance comparison is shown in Figures 1-3 for a 2012 **M4.0** East Prairie, MO earthquake. Figure 1 shows a map of the recording stations for this event along with

the example reference (green) and Q transition boundary crossing (cyan) profiles. Figure 2 presents the 0.2 s and 1.0 s reference profile fits and Figure 3 shows data from a Q transition boundary crossing profile plotted along with the reference profile median and 95% confidence limits curves. At 0.2 s the Q transition boundary clearly is located at an epicentral distance of about 450 km, but at 1.0 s the profile is not long enough, due to the presence of the coast of the Gulf of Mexico, to clearly determine the longer period transition boundary location near 600 km.

East Prairie 2012 Recording Stns

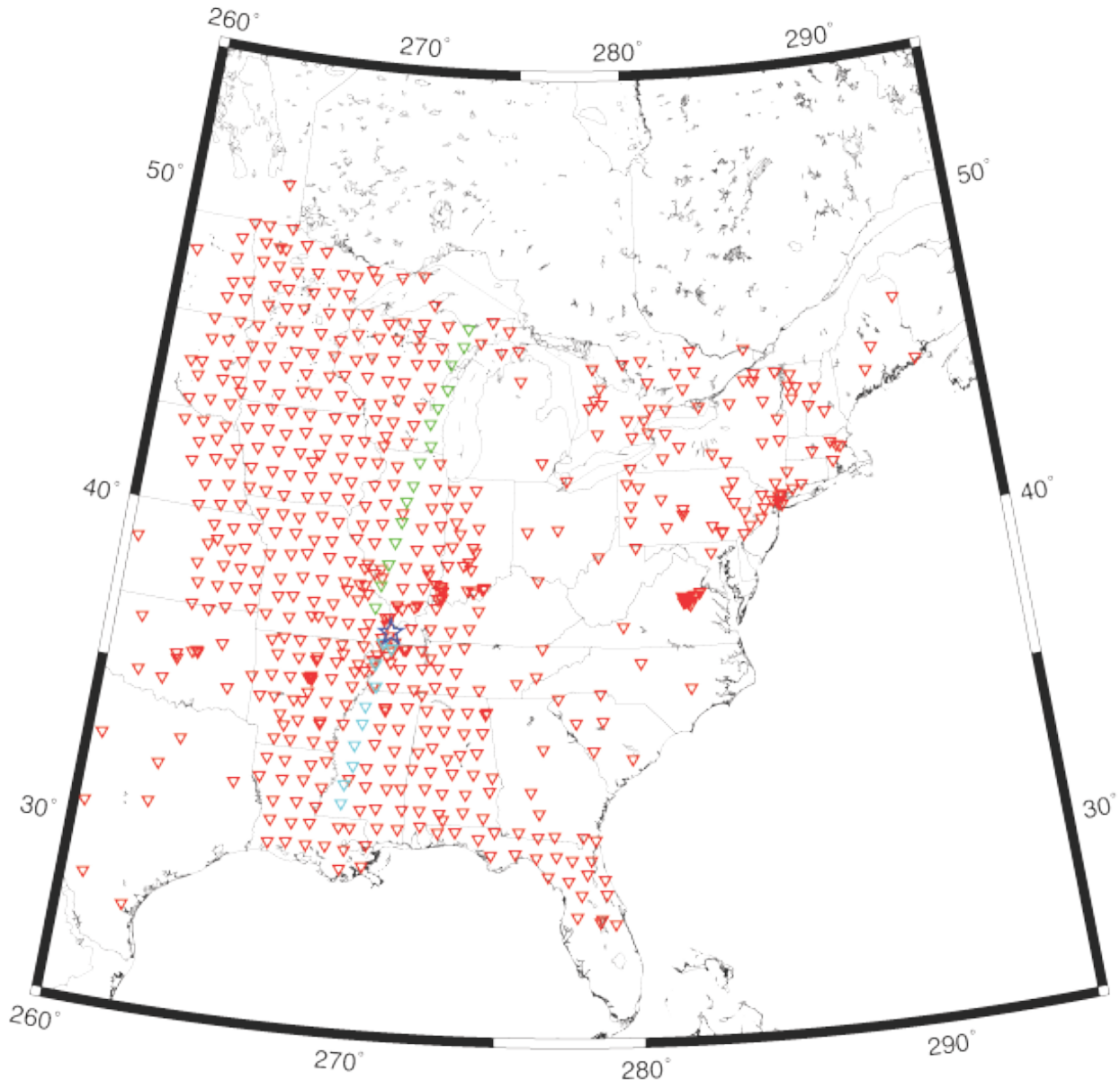


Figure 1: Map of 2012-02-21 M4.0 East Prairie, MO earthquake (blue star), recording stations (inverted triangles), reference profile (green stations), and boundary crossing profile (cyan stations).

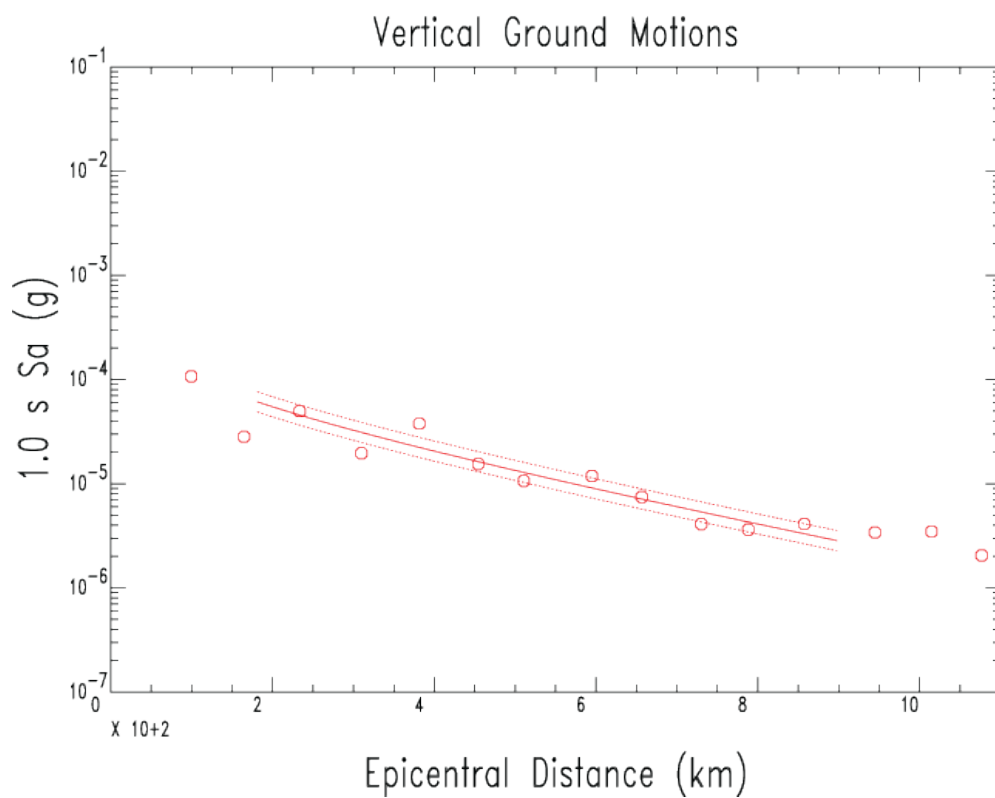
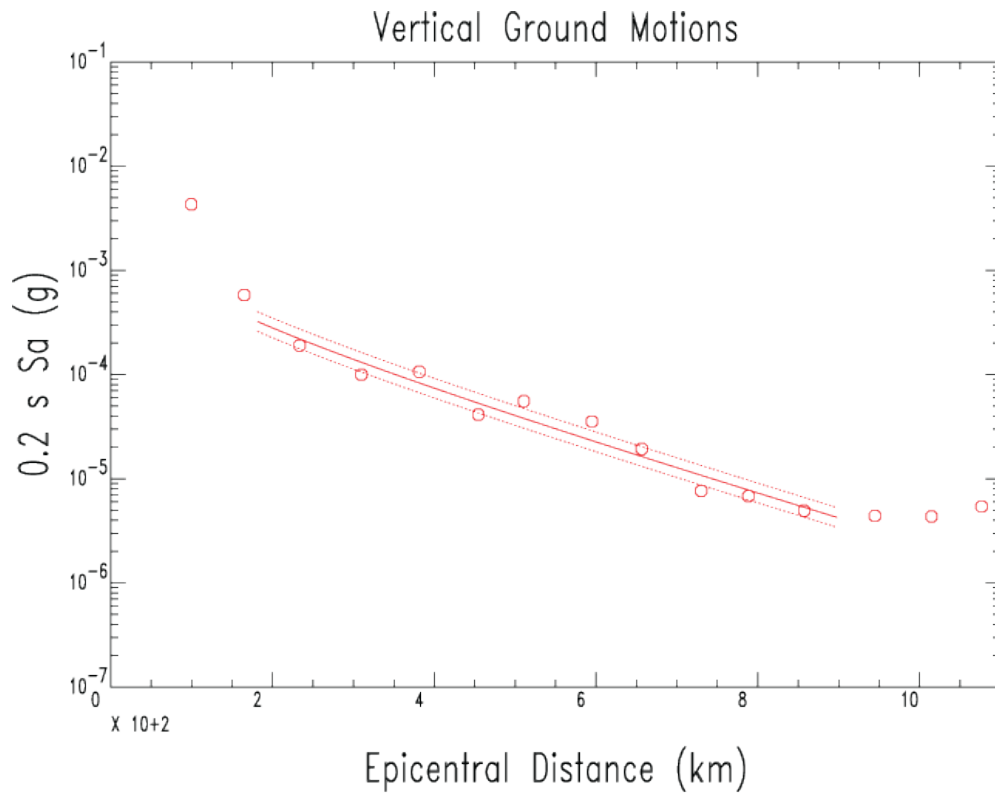


Figure 2: Reference profile and fit (red line) with 95% confidence levels (dotted lines) and observations (red circles) for green profile in Figure 1. Top is 0.2 s and bottom is 1.0 s.

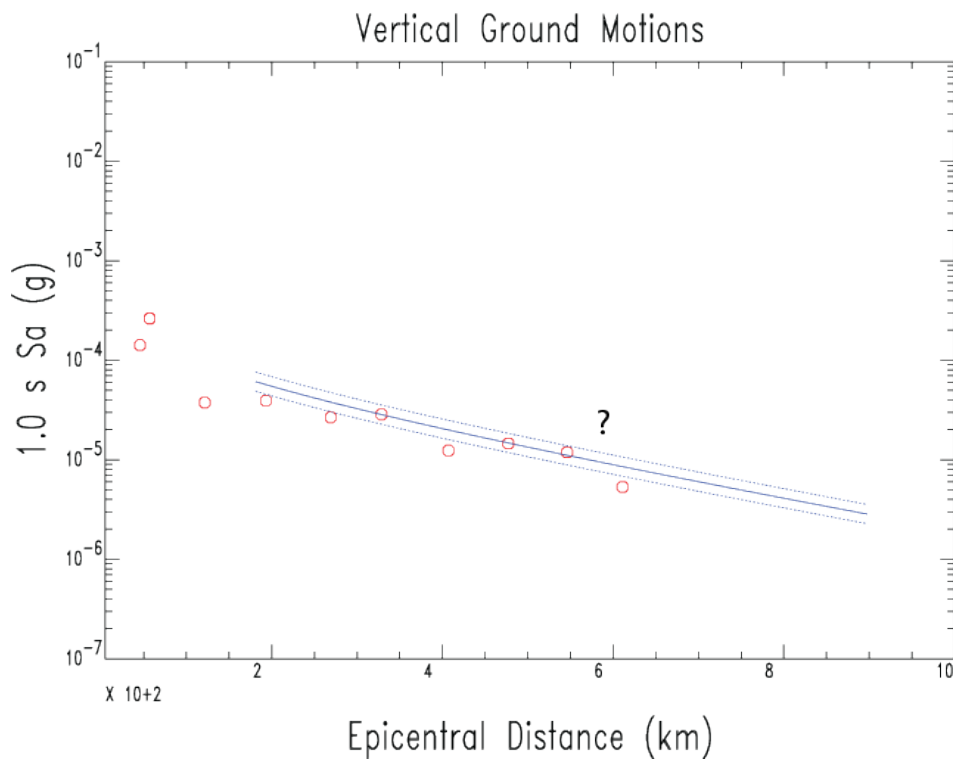
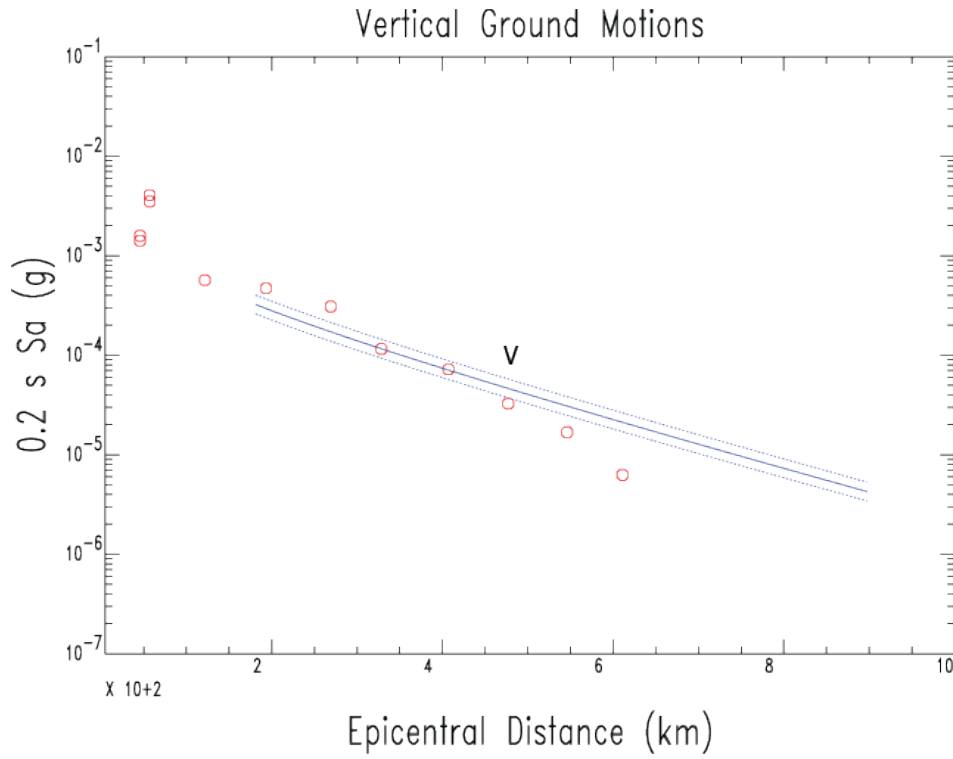


Figure 3: Boundary crossing profile with reference profile from Figure 2 (solid line is mean and dotted line is 95% confidence level). Red circles are observations. Top is 0.2 s and bottom is 1.0 s. Change in attenuation with distance indicated by V and ? symbols.

To aid in visualizing the location of the Q transition boundary at a given frequency (period), we used the reference profile decay trend with distance (Figure 2) to form natural logarithmic amplitude residuals (calculated minus observed) for each station, plot the residuals on a map, and contour the residual in GMT. Figure 4 is an example at 0.2 s for the same earthquake as in Figures 1-3. The negative residuals (cool colors) near the Gulf coast indicate where the 0.2 s higher attenuation is located. However, this approach was not very successful due to amplitude variations due to the strike-slip radiation pattern, propagation effects due to crustal structure, and possibly site geology effects even on vertical component data, particularly to the SE near the Gulf coast in this example. This serves as a warning about the impact of these radiation, propagation, and site effects on observations from individual earthquakes. Tomographic results can also be affected if multiple earthquake raypath sampling is insufficient to cancel out these effects, which can be the case in low seismicity regions.

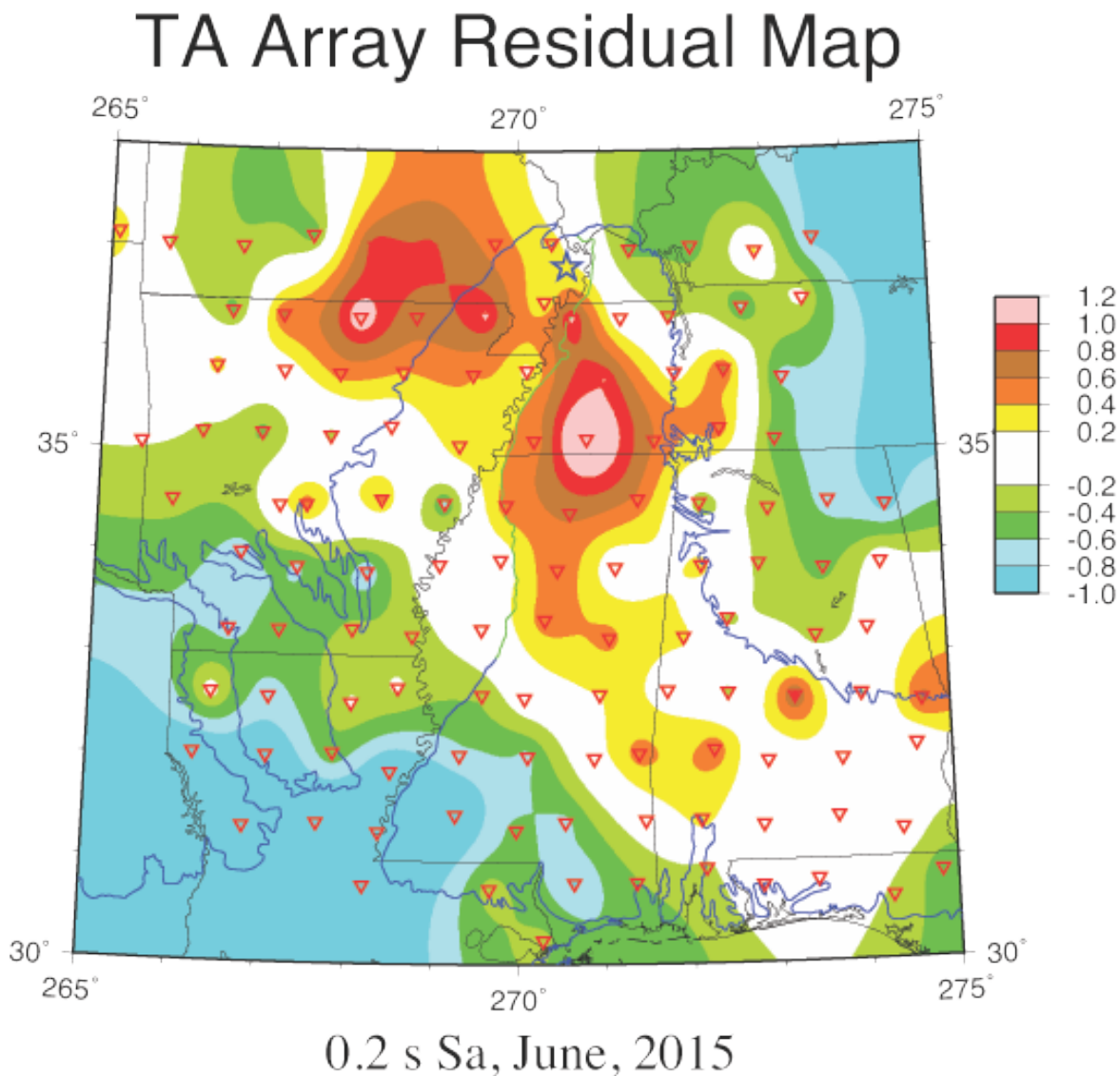


Figure 4: Logarithmic residual map (base 10) relative to reference profile trend in Figure 2 of observations at stations south of the epicenter (blue star) of the 2012 East Prairie MO earthquake.

For individual earthquakes and along a few selected transects we have estimated regional Q using an approach similar to Benz et al. (1997) and Erickson et al. (2004). Our modification is to use narrow bandpass filtering of velocity records to estimate amplitude at a given frequency at each station for a given earthquake. The four-pole Butterworth narrow bandpass center frequencies (f) used are 0.1, 0.13, 0.2, 0.3, 0.4, 0.6, 0.8, 1.0, 1.3, 2.0, 3.0, 4.0, 6.0, 8.0, 10.0, 13.0, and 16.0 Hz with filter corners set $0.025 \log(f)$ below and above the center f (log is logarithm base 10). The filtering was accomplished using SAC (Goldstein et al., 2003). For these estimates we used both horizontal components instead of the vertical component.

Q at frequency f can then be determined from

$$Q(f) = -\pi*f/C*\beta, \quad (2)$$

where C is from the fit to Equation 1 at frequency f and β is crustal shear-wave velocity (3.5 km/s from Benz et al., 1997). All the values of Q at different frequencies can then be fit using

$$\log [Q(f)] = \log (Q_0) + \eta*\log(f), \quad (3)$$

where Q_0 is the Q at 1 Hz and η is the power of f in $Q(f) = Q_0*f^\eta$. Q_0 and η represent the regional Q that can be compared with values from other studies in different regions. All fits are determined by linear least squares inversion (Claerbout, 1976) using the elimination method (Faddeeva, 1959). Regional Q estimates determined in this study are whole record estimates (S and Lg dominate, except at long periods > 5 s where surface waves may dominate in the thicker Gulf Coast sediments) and are similar to the ENA Q estimate approach of Atkinson and Boore (2014) using whole records.

For the Gulf Coast region we define with our Q boundary analysis, we also applied the McNamara et al. (1996) algorithm at each frequency for all the earthquakes and stations within the Gulf Coast region. McNamara's algorithm determines event and site terms as well as Q at a frequency. Frequency dependent Q is then determined from the McNamara Q values at each frequency in the same manner as for an individual earthquake (Equation 3 and linear least squares inversion). Event and station terms are then examined for trends as a function of frequency.

Finally, Gulf Coast GMPEs are developed from a within Gulf Coast dataset using the approach of Al Noman and Cramer (2015). This GMPE determination used the two-stage approach of Joyner and Boore (1993, 1994). This approach provides both within event and between event variability along with event and site terms. The functional form for our regressions is

$$\log Y = f(R) + f(M), \quad (4)$$

where log is a base-10 logarithm. The distance dependent terms are

$$f(R) = (c_1 + c_2M)\log R + c_3(R - R_0) + d_1\log(Vs_{30}/760) + \phi, \quad (5)$$

where R_0 is a reference distance set equal to 1 km, Vs_{30} is the average travel-time Vs for the top 30 meters at the desired location in m/s, and ϕ is the within event variability. The reference

V_{s30} in our regressions is 760 m/s. We have included a magnitude dependent geometrical spreading term to model magnitude saturation at large magnitudes. R_0 does not change the functional behavior of our regression form and provides the added advantage of a reference to ground motion amplitude on hard rock. The magnitude dependent terms of our functional form are

$$f(M) = a_1U + a_2RR + a_3SS + b_1M + b_2M^2 + \tau, \quad (6)$$

where U, RR, and SS are set to one for undefined, reverse, and strike-slip focal mechanisms, respectively, and zero otherwise, and τ is the between event variability. Total variability (uncertainty) σ is given by

$$\sigma^2 = \phi^2 + \tau^2. \quad (7)$$

The distance metric R in the regression is given from the observed rupture distance (R_{rup}) by

$$R^2 = R_{rup}^2 + h^2, \quad (8)$$

where the pseudo-depth term is fixed at 10 km. The value of h could not be determined as an independent variable by the regression and hence arbitrarily fixed at 10 km.

Data

Earthquakes both inside and outside the Gulf Coast region were used in our analysis. At first earthquakes outside the Gulf Coast region were used to look for the transition to increased attenuation within the Gulf Coast region. These earthquakes are listed in Table 1. Then we collected data from earthquakes within or very close to our defined boundary to help refine the location of the boundary and determine how the apparent boundary might shift going from higher to lower attenuation. Table 2 presents these earthquakes. Data with raypaths for these inside events to stations within the Gulf Coast region were used in the regional Q analysis and Gulf Coast GMPE development. We also examined the data from a few earthquakes to the west of the Gulf Coast region for an initial investigation into regional Q there. They are listed in Table 3.

For the Gulf Coast GMPE development we added the data from recordings within 60 km (rupture distance) of the 2010 M7.1 Darfield, New Zealand earthquake to provide control at close-in distances for M7 earthquakes. No such observations exist in the Gulf Coast area. Our Brune stress drop estimate for the Darfield earthquake is 10 MPa, which is comparable to that of the Gulf Coast earthquakes in Table 2. We estimated Q for the Darfield earthquake at distances beyond 50 km and found the frequency dependent Q to have a Q_0 (at 1 Hz) of $106 +15/-13$ with an $\eta = 0.851 \pm 0.045$ (one standard deviation uncertainty). At distances less than 60 km, the effect of this low Q is negligible and the decay with distance is due to geometrical spreading alone and would be valid for any region including the Gulf Coast region of this study. The general geology in the Christchurch, NZ region is similar to the Gulf Coast due to the presence of thick sediment deposits, although not as thick as portions of the Gulf Coast.

Table 1: List of CEUS earthquakes outside the Gulf Coast use to define the Gulf Coast region of high attenuation. Brune stress drop estimates ($\Delta\sigma$) are also provided.

Sullivan, MO 2011-06-07 **M3.9** $\Delta\sigma = 5$ MPa
 Dallas, TX 2011-07-17 **M3.0** $\Delta\sigma = 3$ MPa
 Comal, TX 2011-10-20 **M4.6** $\Delta\sigma = 5$ MPa
 East Prairie, MO 2012-02-21 **M4.0** $\Delta\sigma = 10$ MPa
 Whitesburg, KY 2012-11-10 **M4.2** $\Delta\sigma = 30$ MPa
 Fairview, OK 2016-02-13 **M5.0** $\Delta\sigma = 15$ MPa

Table 2: List of CEUS earthquakes inside or very near the Gulf Coast boundary defined in this report. Individual earthquake estimates of $Q(f)$ is listed after the magnitude of each earthquake. Uncertainties are one standard deviation. Brune stress drop estimates ($\Delta\sigma$) are also provided.

South Texas 2010-04-25 **M3.9** $Q_0 = 211 +40/-33$ $\eta = 1.015 \pm 0.077$ $\Delta\sigma = 0.3$ MPa
 Slaughterville, OK 2010-10-13 **M4.3** $Q_0 = 182 +30/-26$ $\eta = 0.739 \pm 0.063$ $\Delta\sigma = 10$ MPa
 Arcadia, OK 2010-11-24 **M4.2** $Q_0 = 254 +35/-31$ $\eta = 0.569 \pm 0.052$ $\Delta\sigma = 10$ MPa
 Bethel Acres, OK 2010-12-12 **M4.3** $Q_0 = 257 +51/-43$ $\eta = 0.681 \pm 0.048$ $\Delta\sigma = 10$ MPa
 Greenbrier, AR 2011-02-28 **M4.7** $Q_0 = 207 \pm 7$ $\eta = 0.774 \pm 0.018$ $\Delta\sigma = 8$ MPa
 Prague, OK (foreshock) 2011-11-05 **M4.7** $Q_0 = 209 +11/-10$ $\eta = 0.686 \pm 0.026$ $\Delta\sigma = 3$ MPa
 Prague, OK (mainshock) 2011-11-06 **M5.6** $Q_0 = 210 \pm 11$ $\eta = 0.673 \pm 0.027$ $\Delta\sigma = 10$ MPa
 Kiawa, OK 2012-04-03 **M3.8** $Q_0 = 217 \pm 11$ $\eta = 0.608 \pm 0.024$ $\Delta\sigma = 4$ MPa
 Timpson, TX 2012-05-17 **M4.3** $Q_0 = 154 \pm 9$ $\eta = 0.967 \pm 0.020$ $\Delta\sigma = 5$ MPa
 Alabama Coast 2012-11-10 **M2.6** $Q_0 = 187 +95/-63$ $\eta = 1.042 \pm 0.160$ $\Delta\sigma = 0.02$ MPa

Table 3: List of CEUS earthquakes west of the Gulf Coast region defined in this report used for an initial examination of Q in that region. Brune stress drop estimates ($\Delta\sigma$) are also provided.

South Colorado 2010-05-27 **M3.6** $\Delta\sigma = 3$ MPa
 South New Mexico 2010-05-31 **M4.0** $\Delta\sigma = 7$ MPa
 Nebraska 2010-11-18 **M3.3** $\Delta\sigma = 15$ MPa
 Central Texas 2011-09-11 **M4.3** $\Delta\sigma = 5$ MPa

Results

Q Boundary

Figure 5 shows the general coverage of the TA (not all stations were active at the same time) and the initial five outside the Gulf Coast region events and there estimates for the location of the Q transition boundary. Figure 5 demonstrates that the Q boundary is resolvable to within the 70 km grid spacing of the TA stations. Notice that the apparent location for the Q boundary is different for short (PGA, 0.2 s) vs. long periods (1.0 s). This difference in location of the Q boundary as a function of period may be related to the crustal structure within and how earthquake energy propagates into the Gulf Coast region.

Q Boundary & TA Array

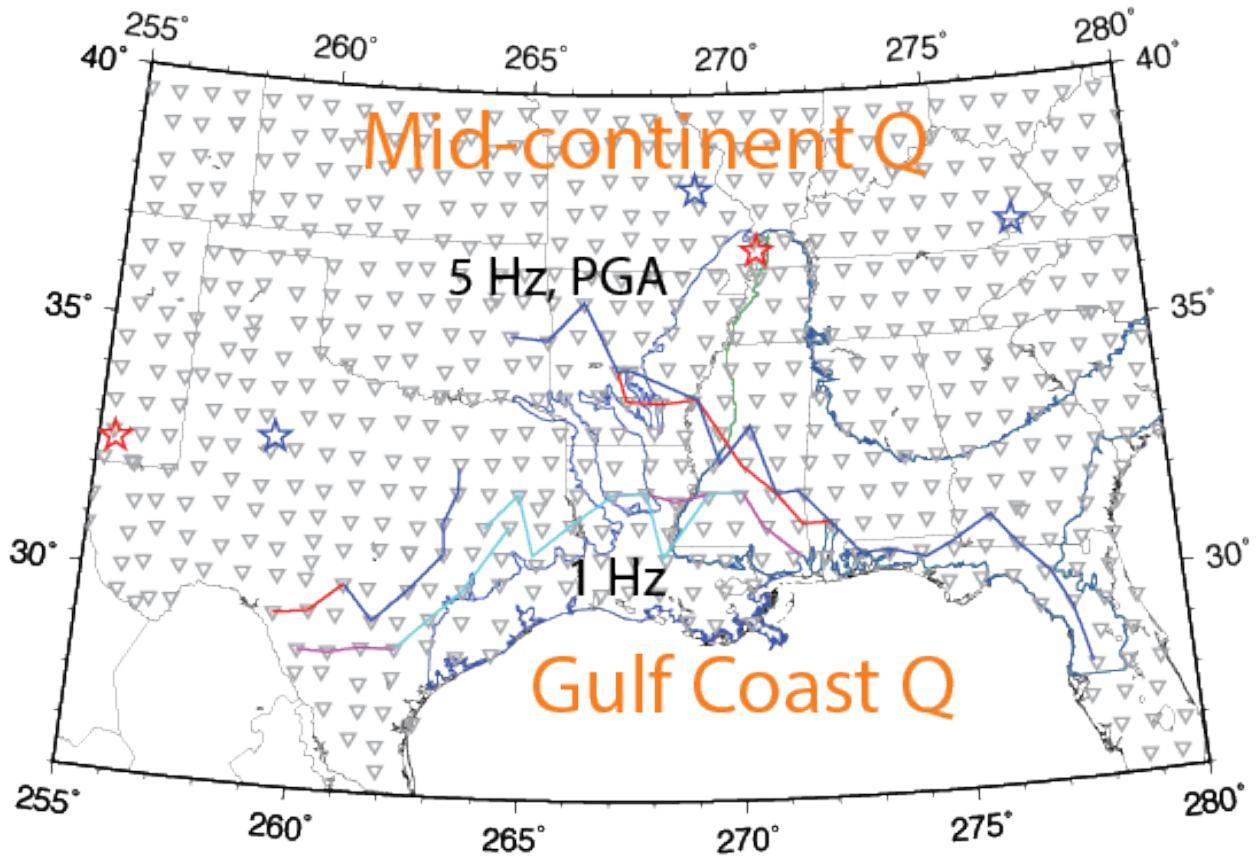


Figure 5: Initial map of Q boundary locations from five earthquakes outside the Gulf Coast Q region. Boundary segments are color coded to alternating earthquake colors: red (short period) and magenta (long period) for red star earthquakes and blue and cyan for blue star earthquakes. Thin blue lines indicate boundary of coastal sediments and thin green line in embayment denotes lowlands (west) from uplands (east). Grey inverted triangles are USArray stations.

Figure 6 shows the initial location of the Q transition in the eastern portion of the Gulf Coast region from two events inside the Gulf Coast region. Again the boundary resolution is the 70 km spacing of the TA array. Also the boundary does seem shifted northeast of the location from the outside earthquakes in Figure 5, possibly due to crustal structure and wave propagation differences between the regions. The sparse seismicity in the CEUS limits the number of earthquakes available to help resolve the Q boundary location.

Figure 7 and Tables 4 and 5 present our final location of the boundary between mid-continental and Gulf Coast Q . It is established from the data for the earthquakes in Tables 2 and 3, except the recent Fairview, OK $M5.0$ and the older South Texas $M3.9$ earthquakes. We consistently see the indicated different locations of this transition boundary for short and long period for earthquakes outside the Gulf Coast Q region similar to what is shown in Figure 3, but not within the Gulf Coast region. In northern Texas and southern Oklahoma, we have dashed the boundary

location because it is not well resolved there, possibly due to other tectonic features merging with the Gulf Coast region (see further discussion below in the Regional Q section).

Q Boundary & TA Array

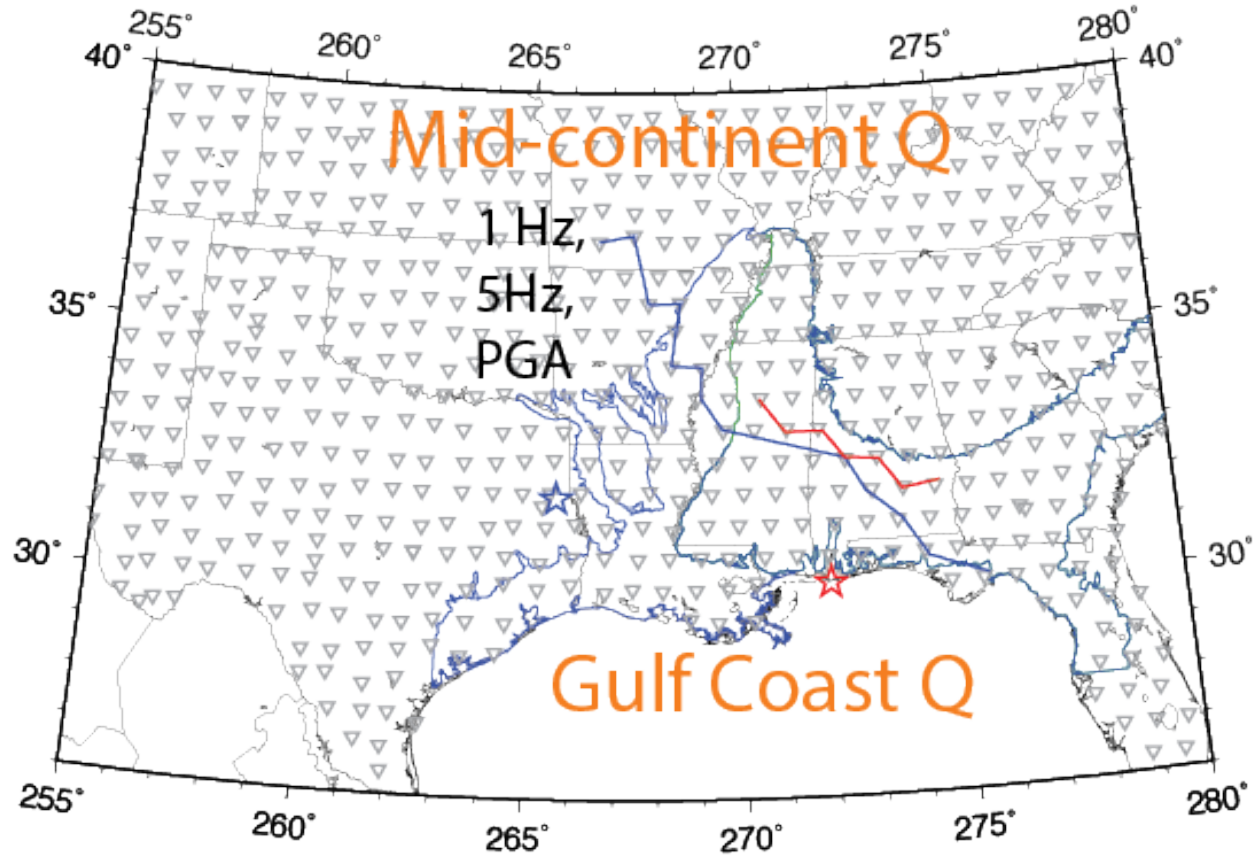


Figure 6: Initial map of Q boundary location from two earthquakes within the Gulf Coast region. Color coding and symbols are the same as in Figure 5.

Q Boundary & TA Array

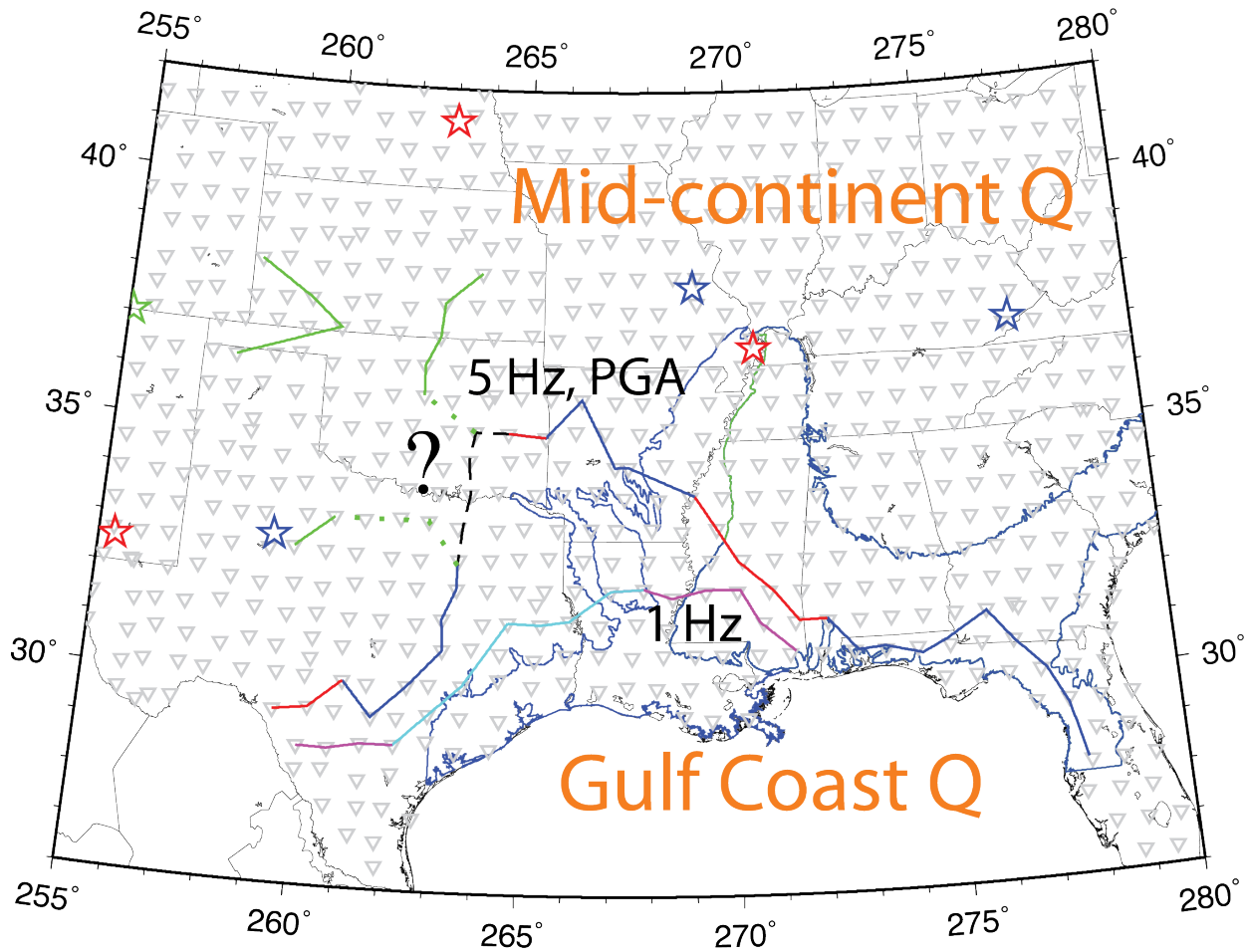


Figure 7: Final map of Q boundary locations from earthquakes outside the Gulf Coast region. Color coding and symbols are the same as in Figure 5 with the addition of the green boundary lines west of the Gulf Coast region from the green earthquake in southern Colorado. The dashed Gulf Coast boundary is where other crustal Q structures intersect it. The dotted lines are speculative connections between Gulf Coast and crustal structures further west. The question mark emphasizes uncertainty in boundary locations in that region.

Figure 8 presents this final location of the boundary with respect to earthquakes within and near the boundary and the fact that the short and long period boundary location is the same for events within the Gulf Coast region. The near the boundary events in central Oklahoma and Arkansas clearly show within Gulf Coast Q along path azimuths heading into the Gulf Coast region, suggesting crustal structures that connect with the Gulf Coast Q region, particularly in Oklahoma.

The tectonic setting of Thomas (2010) is shown in Figure 9. Note that our location of the Gulf Coast attenuation region seems somewhat coincident with Thomas' Oklahoma-Alabama transform and the Oachita thrust. Our location of the boundary in Oklahoma extends more into central Oklahoma than Thomas' interpretation, possibly due to other rift structures connecting

with the Gulf Coast low Q region. Thomas indicates that there is major crustal thinning in the Gulf Coast region.

Q Boundary & TA Array

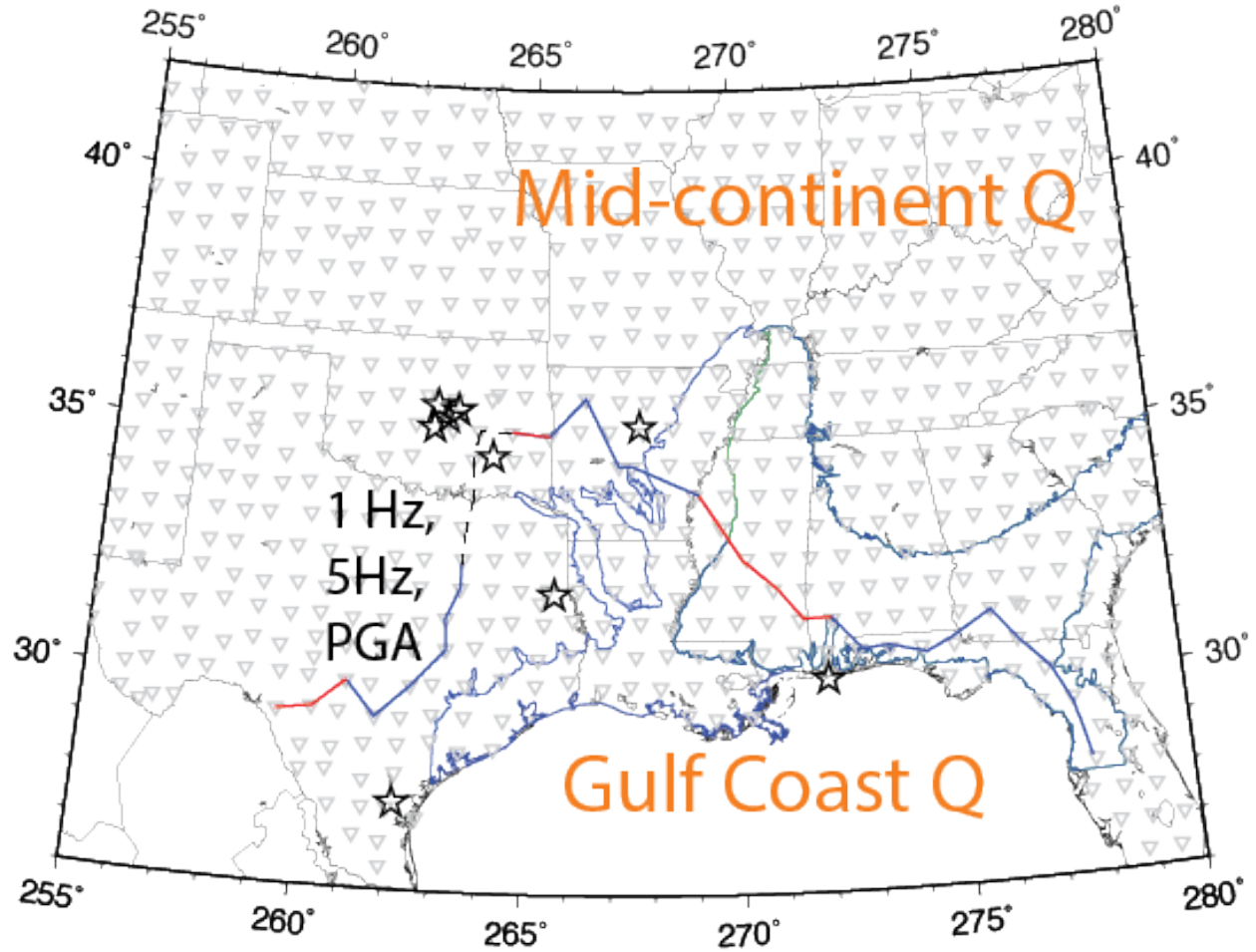


Figure 8: Final map of Q boundary for earthquakes within and near the Gulf Coast region. The Gulf Coast boundary is from Figure 7 and the black stars are earthquakes that exhibit Gulf Coast Q for raypaths within the Gulf Coast region.

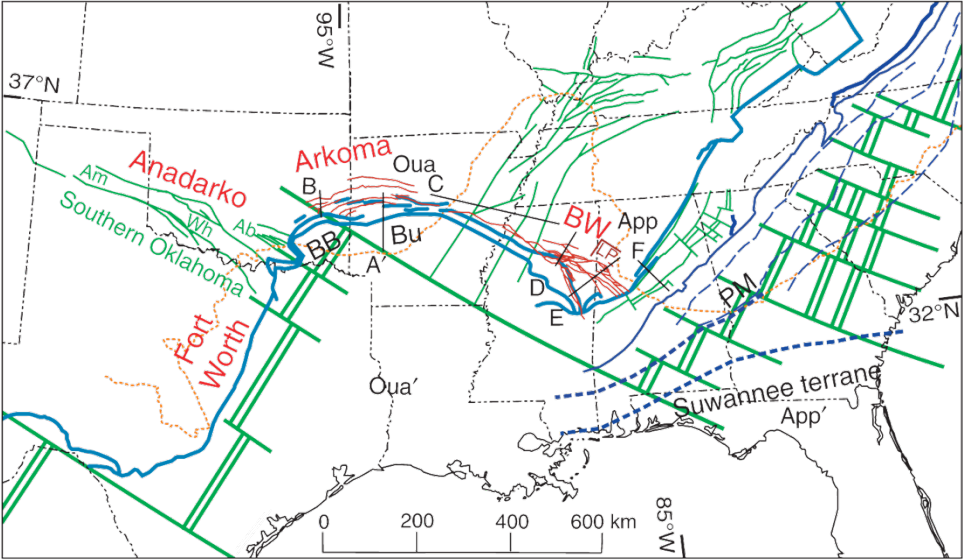


Figure 9: Tectonic setting from Thomas (2010).

Table 4: Coordinates of final Q boundary between mid-continent and Gulf Coast Q regions at short periods for earthquakes outside the Gulf Coast region and all periods within the Gulf Coast region. The boundary is set at the closest TA station (listed) to the observed change in slope of ground motion decay with distance as the uncertainty is on the order of the TA spacing of 70 km. The dashed line between the northern and western segments in Figures 7 and 8 connects the nearest end points in the table through TA station W36A (-96.22640, 35.13930).

Northern Boundary:

Longitude	Latitude	Station
-82.22910	28.26700	TA.857A
-82.53480	29.36890	TA.656A
-82.96660	30.12120	TA.555A
-83.63020	30.71450	TA.454A
-84.21720	31.34740	TA.353A
-85.18300	30.84920	TA.452A
-85.74670	30.61600	TA.451A
-86.58630	30.80380	TA.450A
-87.21510	30.75960	TA.449A
-87.90230	31.41290	TA.348A
-88.54120	31.40170	TA.347A
-89.12860	32.01430	TA.246A
-89.92870	32.60350	TA.145A
-90.43220	33.27730	TA.Z44A
-90.92850	33.91210	TA.Y43A
-92.51370	34.49490	TA.X41A
-92.83420	34.48730	TA.X40A
-93.64500	35.83890	TA.V39A
-94.51840	35.07040	TA.W38A
-95.43160	35.13900	TA.W37B

Western Boundary:

Longitude	Latitude	Station
-96.52970	32.47460	TA.136A
-96.53100	31.99970	TA.236A
-96.84430	31.38700	TA.336A
-96.79600	30.77020	TA.436A
-97.57110	30.02900	TA.535A
-98.35150	29.38150	TA.634A
-99.03510	30.07180	TA.533A
-99.78630	29.50710	TA.632A
-100.57590	29.41230	TA.631A

Table 5: Coordinates of final Q boundary between mid-continent and Gulf Coast Q regions at long periods for earthquakes outside the Gulf Coast region. The boundary is set at the closest TA station (listed) to the observed change in slope of ground motion decay with distance as the uncertainty is on the order of the TA spacing of 70 km.

Longitude	Latitude	Station
-88.65420	30.79520	TA.447A
-89.46490	31.38760	TA.346A
-89.89580	32.03220	TA.245A
-90.68560	32.04220	TA.244A
-91.48270	31.88030	TA.243A
-92.15210	32.06170	TA.242A
-92.91880	32.02270	TA.241A
-93.88960	31.41670	TA.340A
-94.55600	31.33310	TA.339A
-95.31060	31.35670	TA.338A
-96.31550	30.07990	TA.537A
-97.05700	29.48100	TA.636A
-97.80810	28.85530	TA.735A
-98.55760	28.84730	TA.734A
-99.29390	28.71920	TA.733A
-99.97070	28.72920	TA.732A

Regional Q

Within Gulf Coast Region

As noted in Table 2, the frequency dependent Q within our Gulf Coast region has been determined from bandpassed filtered observations for individual earthquake datasets. Generally Q_0 (Q at 1 Hz) ranges from 150 to 250, which is considerably lower than mid-continental Q_0 of around 525 for whole waveform observations (Atkinson and Boore, 2014) and similar to western North America Q_0 values (Benz et al. 1997; Erickson et al., 2004). In Table 2 there is a trend for Q_0 to be below 200 for paths in the eastern half of the Gulf Coast region (Louisiana, Mississippi, southernmost Alabama) and above 200 for paths in the western half.

Using the data from the earthquakes in Table 2 for earthquakes and paths inside our defined Gulf Coast region, we used McNamara's approach and code to estimate Q at various frequencies within Gulf Coast. Figure 10 shows the regional trend that results when event and station terms are considered in the inversion. The within Gulf Coast regional $Q(f)$ is $Q_0 = 259 +24/-22$ and $\eta = 0.715 \pm 0.013$ over a broad frequency band of 0.1 to 16 Hz. Error estimates are one standard deviation. For a narrower frequency band of 1.0 to 16 Hz, Figure 10 also shows a $Q(f)$ fit of $Q_0 = 232 +19/-18$ and $\eta = 0.778 \pm 0.027$, which agrees with the broader frequency band fit within uncertainty. An analysis of the frequency dependent site terms show a large variation across the Gulf Coast region at long periods (> 5 s) and smaller variations at short periods (< 1 s) as shown

in Figure 11. This trend in station corrections is related to the increasing sediment thickness to greater than 10 km toward the coast of the Gulf of Mexico (Chapman and Conn, 2016).

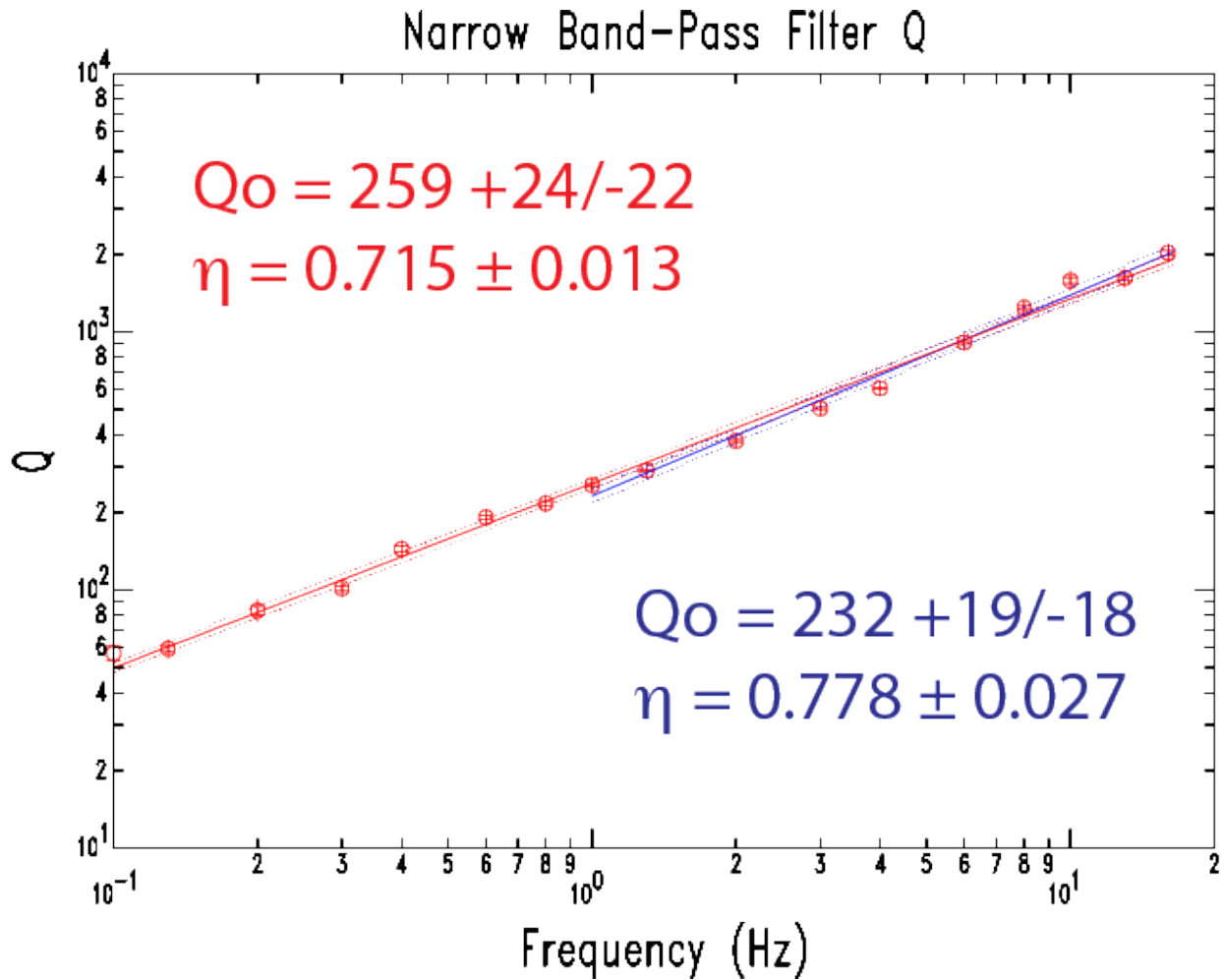


Figure 10: $Q(f)$ fits to McNamara method determined Q values as a function of frequency for raypaths within the Gulf Coast region (red circles with 95% confidence interval + marks). Red lines (solid - mean, dotted - 95% confidence levels) and Q_0 and η values are for fit over 0.1 to 16 Hz. Blue lines and values are for fit from 1 to 16 Hz. Errors in Q_0 and η are one standard deviation values.

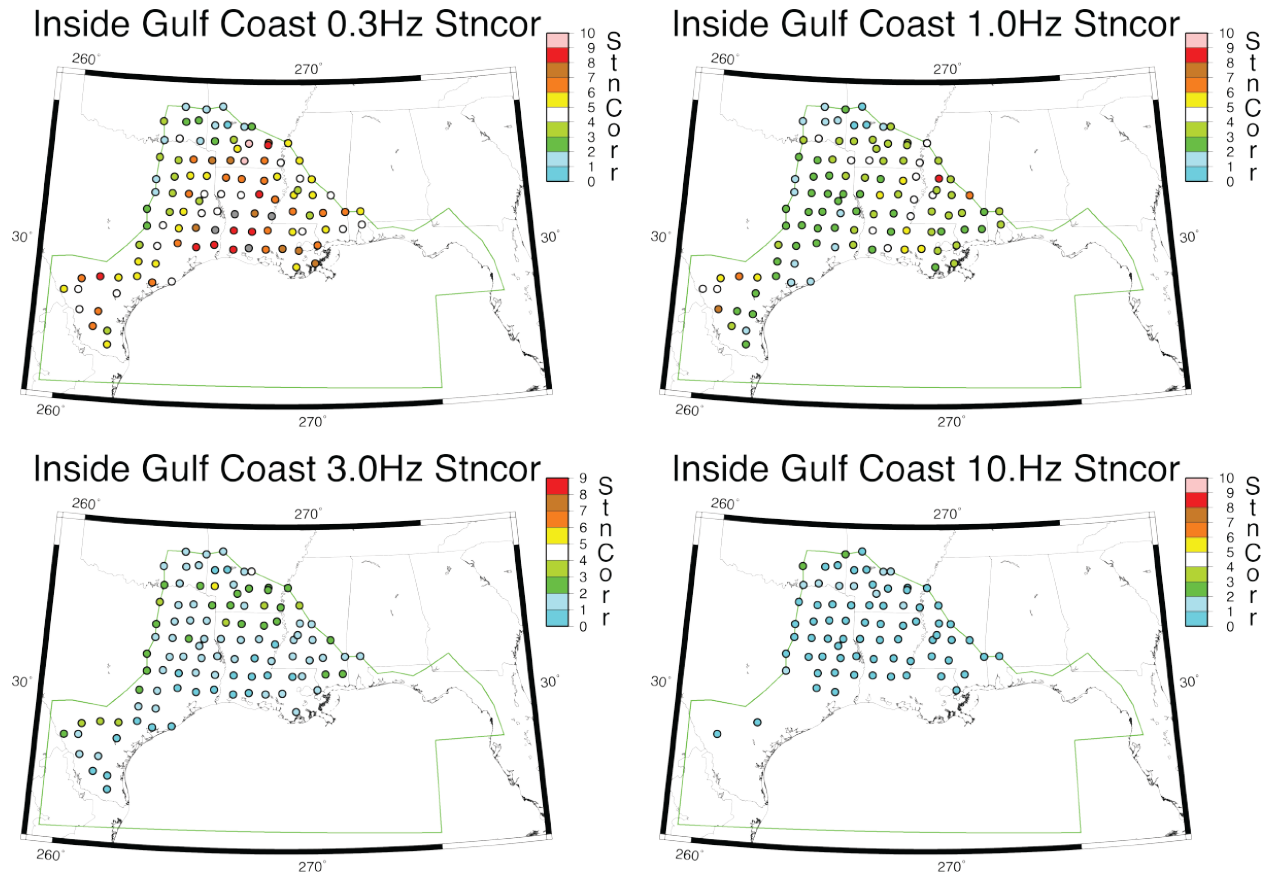


Figure 11: Maps of station corrections from McNamara method for Q values in Figure 10 at 0.3, 1.0, 3.0, and 10 Hz.

Florida Peninsula

The Florida Peninsula has generally been associated with the Gulf Coast attenuating region in past regionalizations for hazard analysis based on seismotectonic regions (EPRI, 1993) and crustal velocity profiles (Dreiling et al., 2014). Dreiling et al. (2014) shows the Atlantic Coastal Plain to be a separate Q region with $Q(f)$ similar to mid-continental Q . Our Q boundary analysis above shows the Florida Peninsula to be outside the Gulf Coast Q region (Figure 7). We used the 2014 **M**4.2 Whitesburg, KY and the 2014 **M**5.0 Northern Cuba earthquakes to examine the crustal Q of the Florida Peninsula.

Figure 12 shows the location of the Whitesburg, KY earthquake and the stations to the south used in a single event Q analysis for eastern Georgia and the Florida Peninsula. A profile of stations to the NW of the epicenter in the mid-continental Q region was used as a mid-continental attenuation reference in the analysis. Figure 13 is the single event $Q(f)$ plot for the reference profile to the NW and shows a $Q_0 = 568 + 88/-76$ and $\eta = 0.66 \pm 0.06$, which is typical mid-continental Q .

Whitesburg KY 2012 Profile 6 Stns

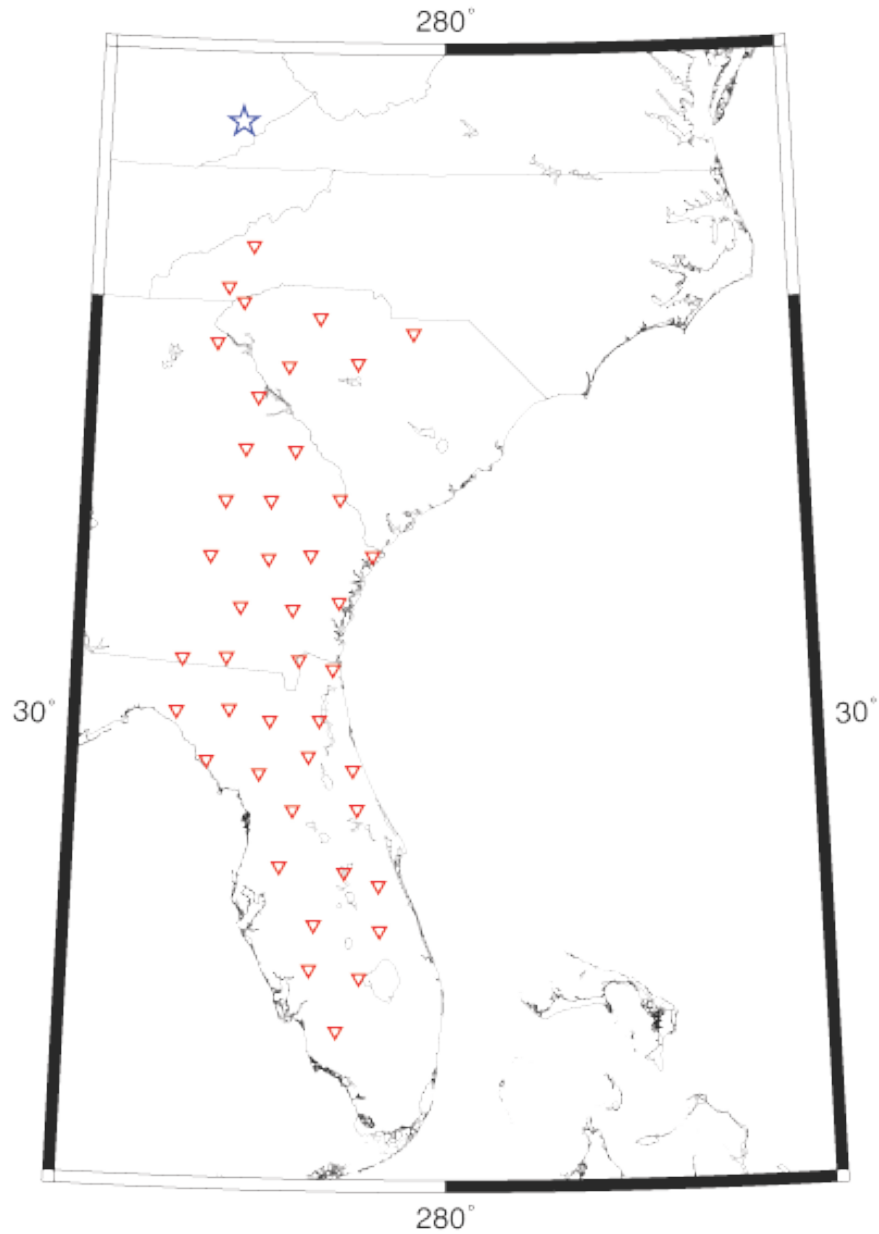


Figure 12: Map of 2012 M4.2 Whitesburg KY earthquake recordings used in Florida Peninsula Q analysis. Blue star is epicenter and red inverted triangles are recording stations used.

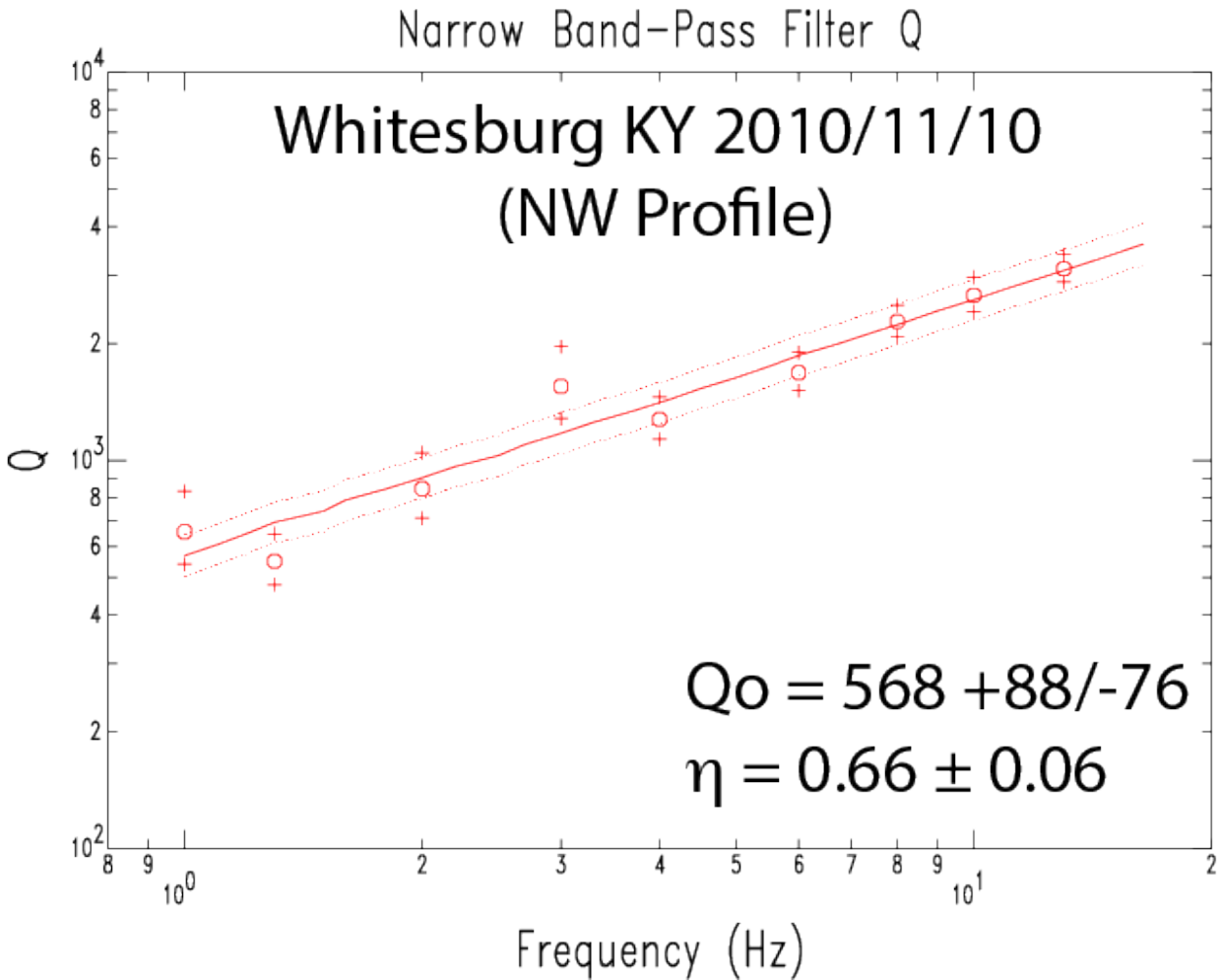


Figure 13: Individual earthquake $Q(f)$ plot for stations along the NW mid-continental Q profile. Red lines are mean fit (solid) and 95% confidence interval (dotted). Red circles are mean Q values for each frequency with + above and below indicating 95% confidence level.

Figure 14 presents the 0.2 s and 1.0 s amplitudes with distance along the Georgia/Florida profile. Clearly the attenuation with distance is very similar to the mid-continental reference shown in Figure 14 for comparison and hence unlike the more attenuating Gulf Coast regional Q . Near the Georgia/Florida border the 0.2 s profile shows a small systematic step-down in the attenuation trend, possibly associated with the clastic/limestone transition in sediments in that area. This step-down does not appear in the 1.0 s trend. Figure 15 shows the $Q(f)$ plot for the Georgia/Florida profile. $Q_0 = 720 + 38/-36$ and $\eta = 0.22 \pm 0.04$ for this profile. A constant Q model of about 1000 can also be fit to this trend.

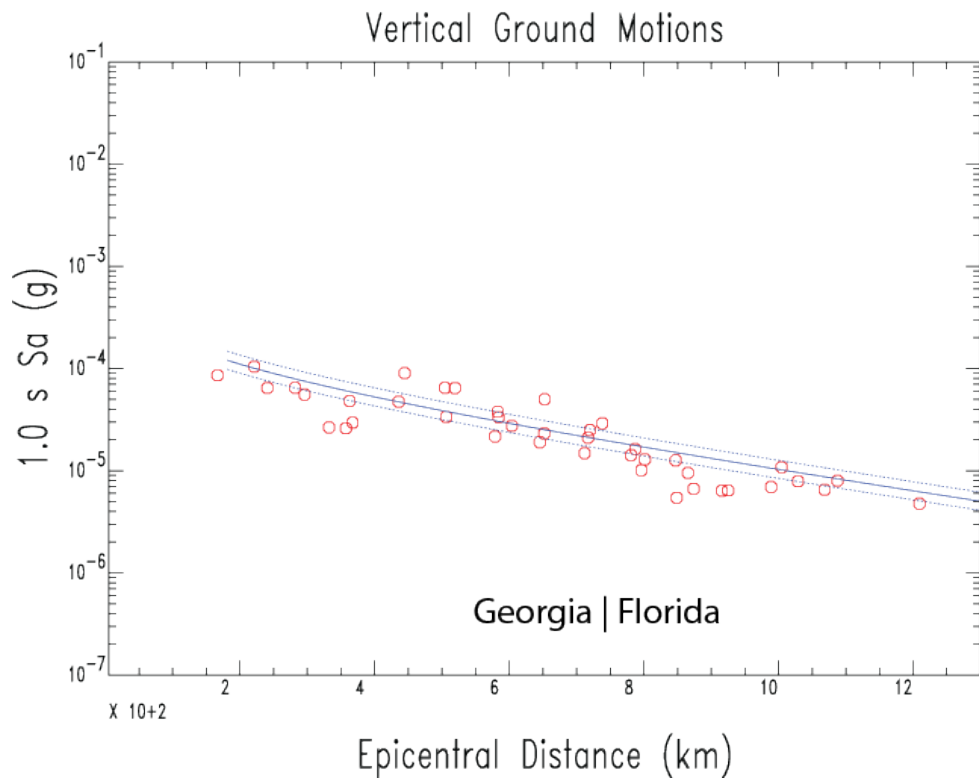
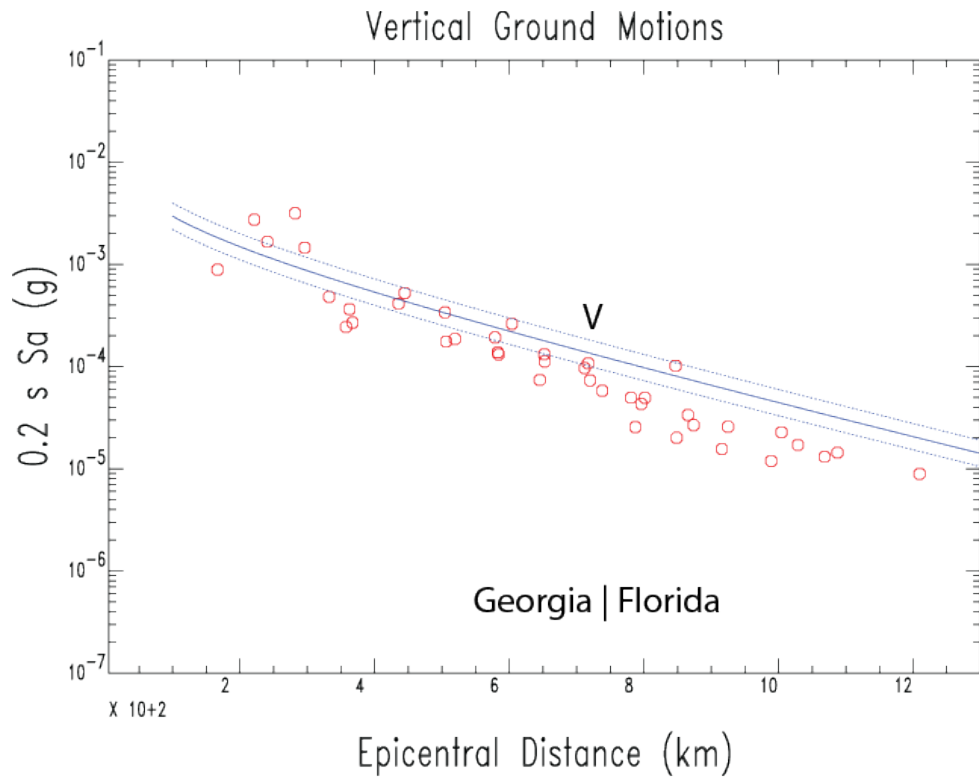


Figure 14: Decay of ground motion amplitude with distance for the stations in Figure 12 at 0.2 s (top) and 1.0 s (bottom). Red circles are observations. For reference the solid line is the mean and dotted lines are the 95% confidence limits of decay with distance fit for the mid-continental Q profile to the NW of the epicenter. V indicates the location of the offset in the 0.2 s values.

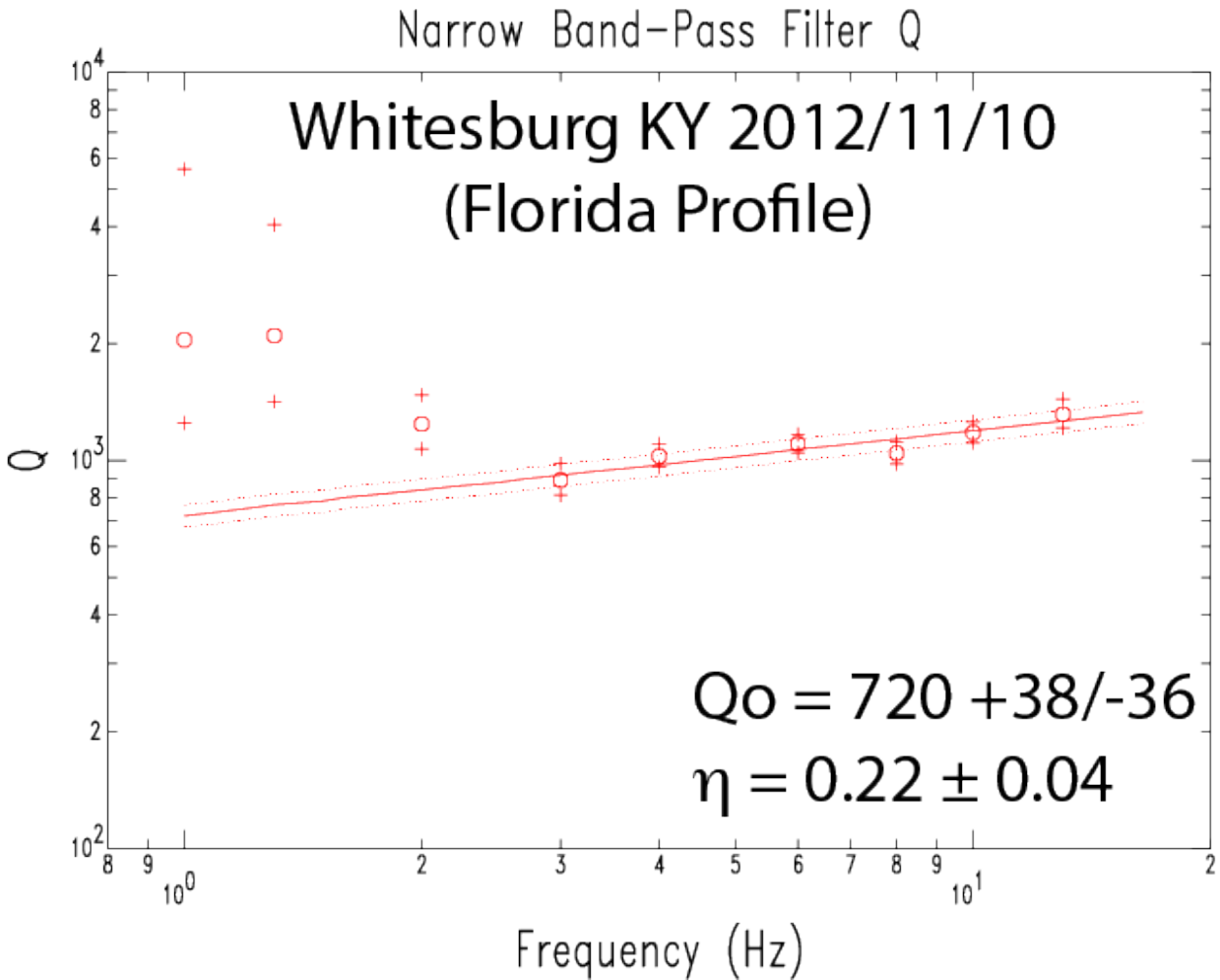


Figure 15: Individual earthquake $Q(f)$ plot for stations in Figure 12. Lines and symbols have the same meaning as in Figure 13.

Figure 16 shows the location of the 2014-01-09 $M_{5.0}$ North Cuba earthquake and the Florida stations that recorded it. The station coverage in Florida is reduced as most to the USArray stations had been removed by the time of that earthquake. Figure 17 presents the $Q(f)$ plot for the Cuba earthquake and shows a constant $Q = 1939 +823/-578$. Thus our Kentucky and Cuba earthquake Q estimates suggest a constant Q for the Florida Peninsula in the 1000 to 2000 range, which at high frequencies is more attenuating than the typical mid-continental $Q(f)$ and at all frequencies is different from Gulf Coast $Q(f)$.

Cuba 2014 Recording Stns

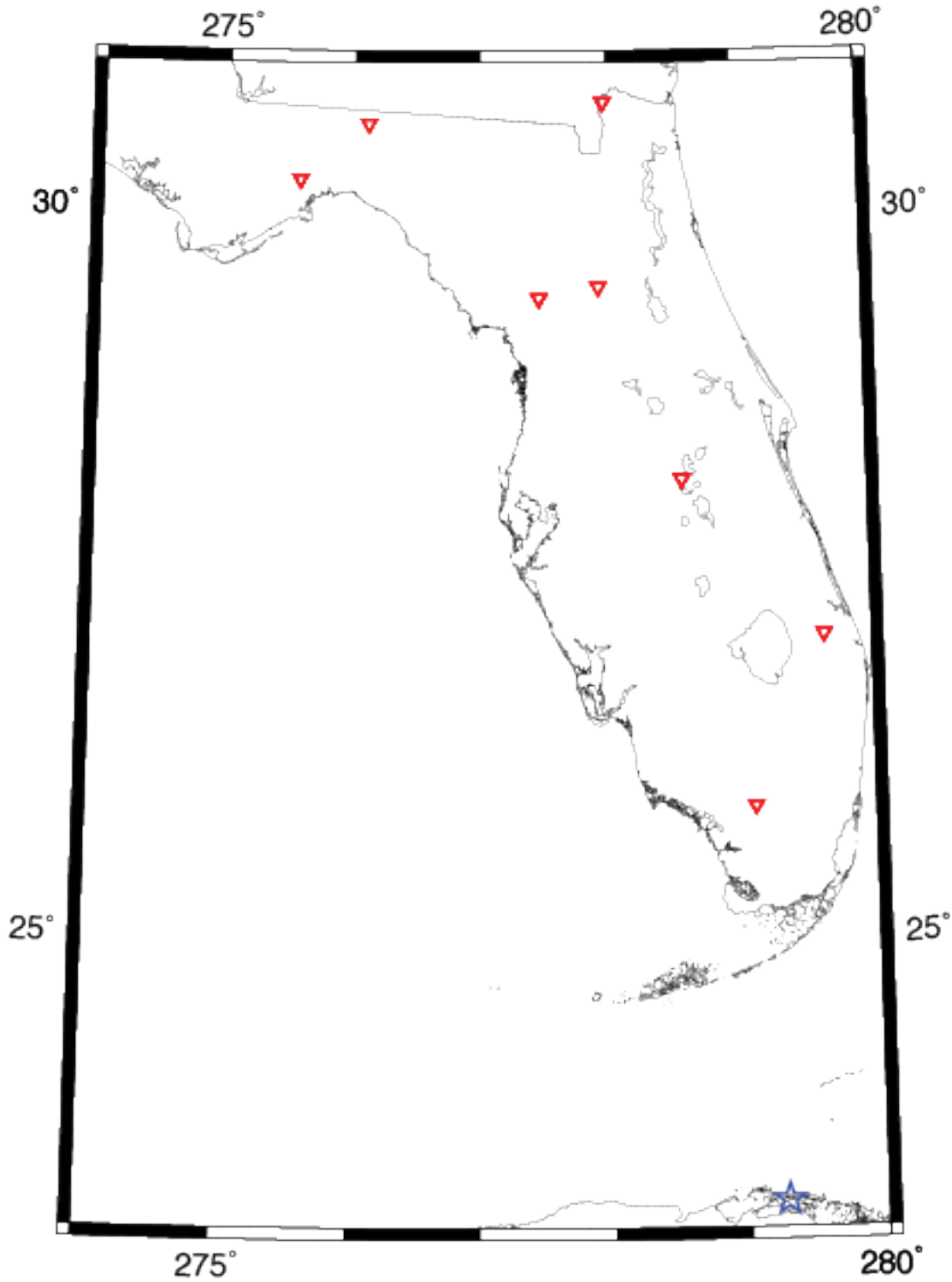


Figure 16: Map of epicenter (blue star) and stations in Florida (red inverted triangles) for the 2014 $M5.0$ North Cuba earthquake.

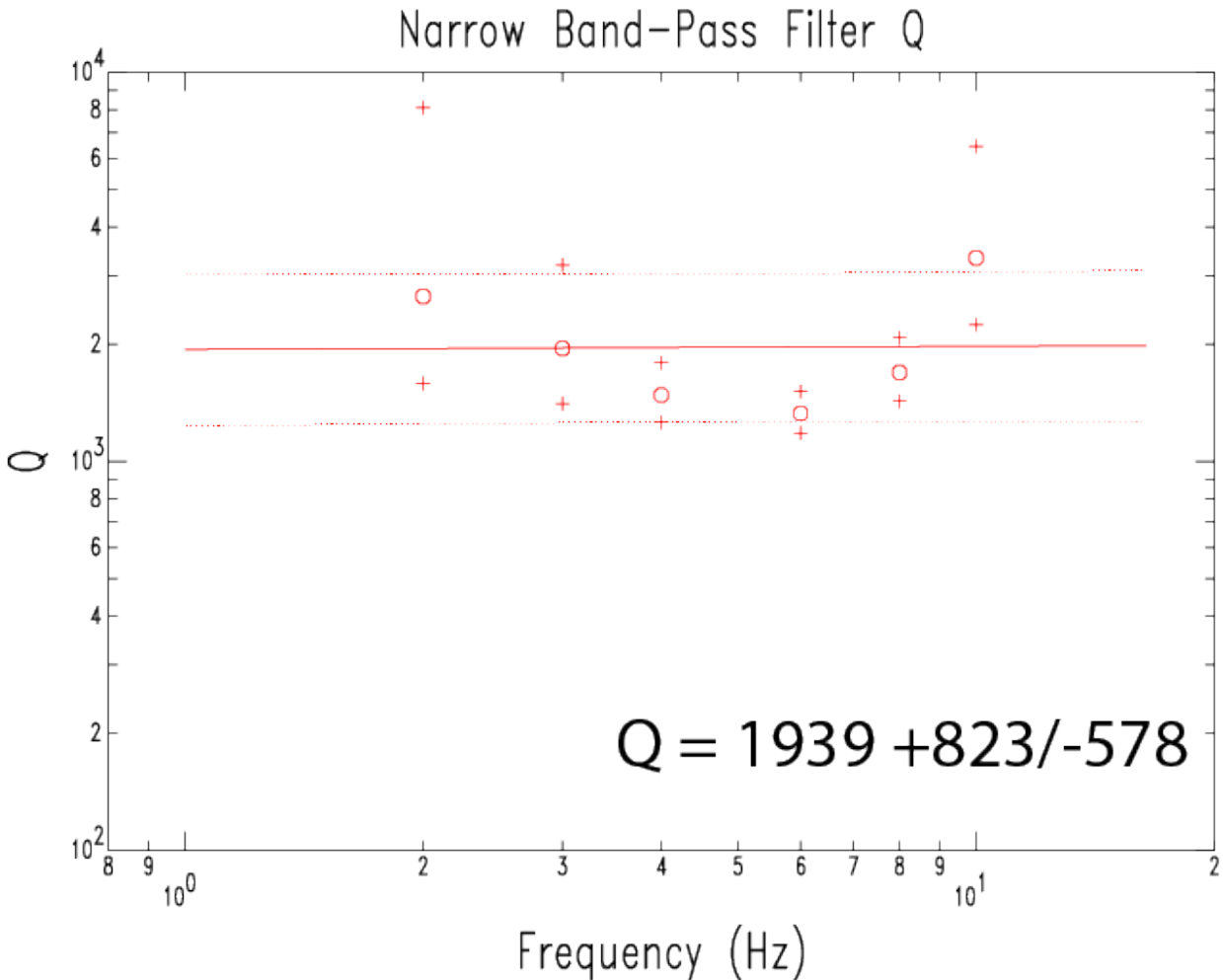


Figure 17: Individual earthquake $Q(f)$ plot for stations in Figure 16. Lines and symbols have the same meaning as in Figures 13 and 15.

Q West of the Gulf Coast

As indicated in Figure 7, there is a complication in the crustal Q structure in south central Oklahoma and northern Texas and to the west that are not well resolved by this current study. Figure 18 shows the stations used in our study for the 2010 **M**3.3 Nebraska earthquake. Higher Gulf Coast attenuation truncates observations to the south in east Texas but observations extend further south in west Texas due to less attenuation in that region. Figure 19 shows the $Q(f)$ results for a profile through Oklahoma/Texas with $Q(f)$ along the profile of $Q_0 = 344 +59/-51$ and $\eta = 0.761 \pm 0.062$. This $Q(f)$ falls between mid-continental and Gulf Coast Q . On the other hand, Q along a profile to the SE of the 2010 **M**3.6 earthquake in Southern Colorado (Figure 20) passing through the Oklahoma/Texas border region shows a $Q(f)$ with $Q_0 = 244 +81/-61$ and $\eta = 0.873 \pm 0.134$ (Figure 21), which is similar to our Gulf Coast Q .

This azimuthal dependence may be due to east-west crustal structures such as the southern Oklahoma rift shown by Thomas (2010) (Figure 9) having less influence on north-south profiles than east-west profiles. The dimensions of these structures make them harder to resolve with the 70 km spacing of the USArray. Additionally, as indicated in Figure 7 by the results of the

Southern Colorado earthquake (green lines) the basins east of the eastern front of the Rocky Mountains may have a low Q signature at higher frequencies. Further study is needed to resolve these low Q at higher frequency (5 Hz) features west of our Gulf Coast low Q region, including how they might interconnect. Interestingly, at low frequency (1 Hz) we always observe high Q mid-continental attenuation, much like the difference in Q boundary locations at these frequencies for earthquakes outside the Gulf Coast region.

E Nebraska 2010 Recording Stns

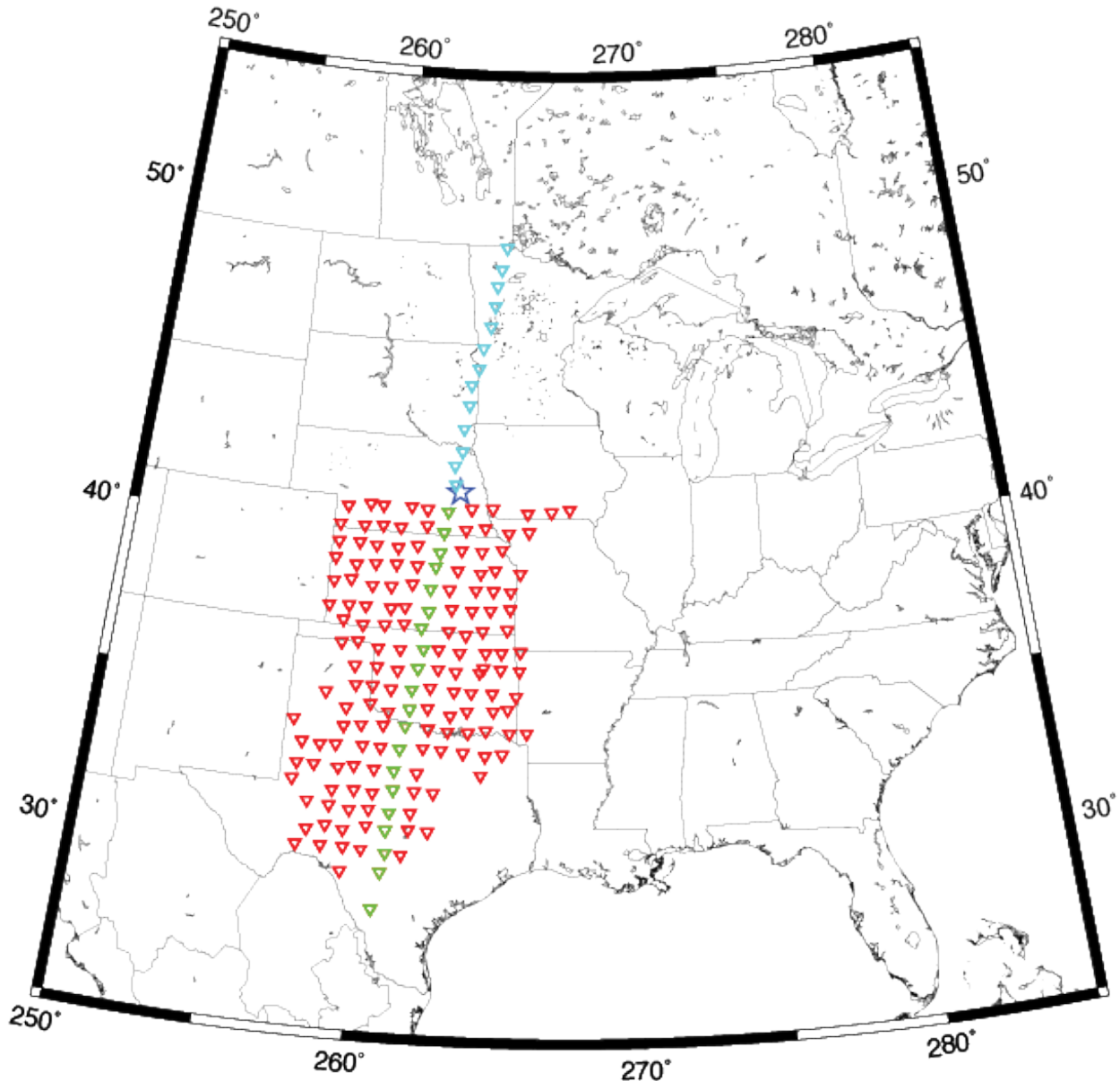


Figure 18: Map of epicenter (blue star) and stations examined (inverted triangles) for the 2010 M3.3 Nebraska earthquake. Green stations form the southern profile through the Kansas, Oklahoma, and Texas region. The cyan profile is a mid-continental Q reference profile.

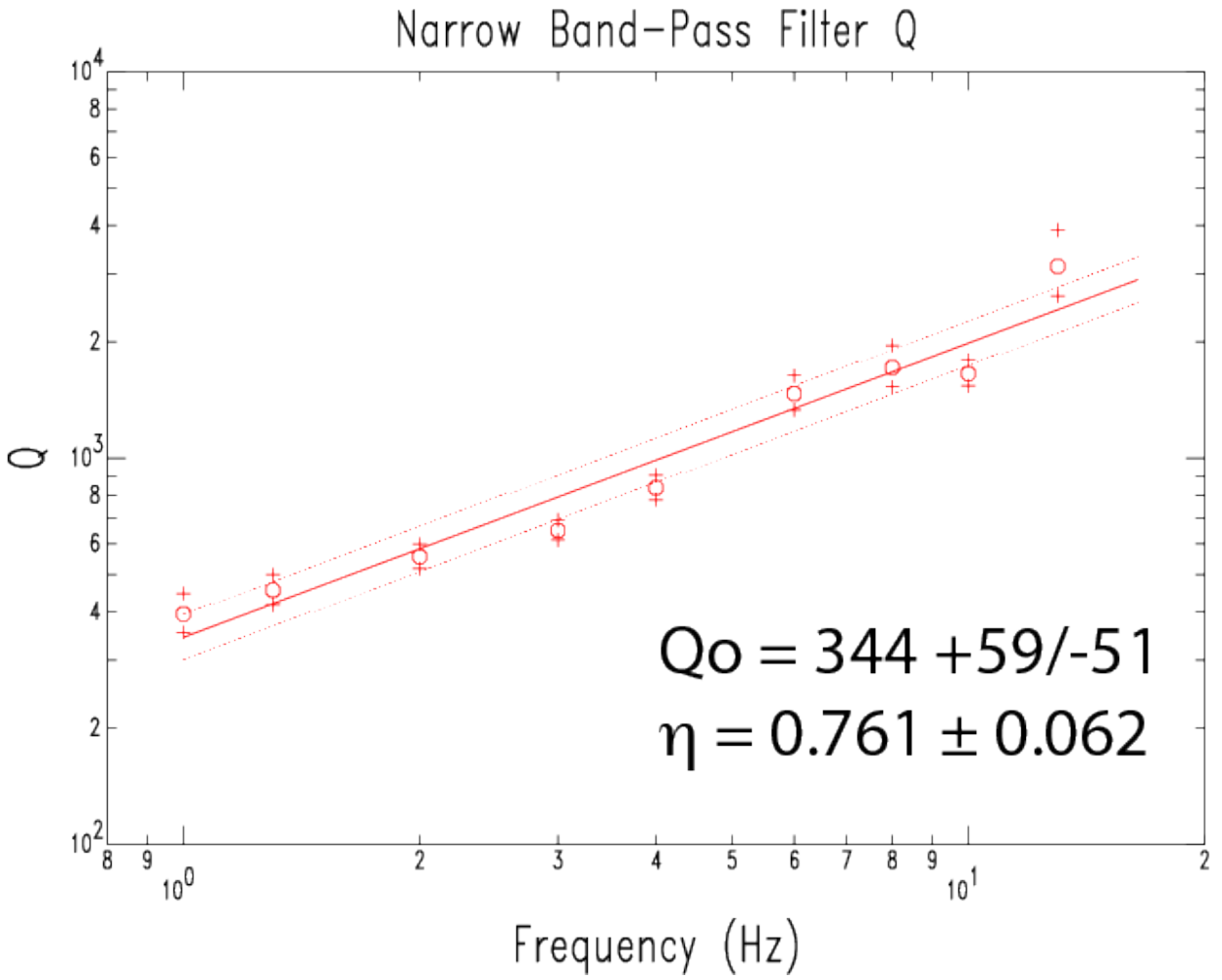


Figure 19: Individual earthquake $Q(f)$ plot for the green profile in Figure 18. Lines and symbols have the same meaning as in Figures 13 and 15.

Colorado S 2010 Recording Stns

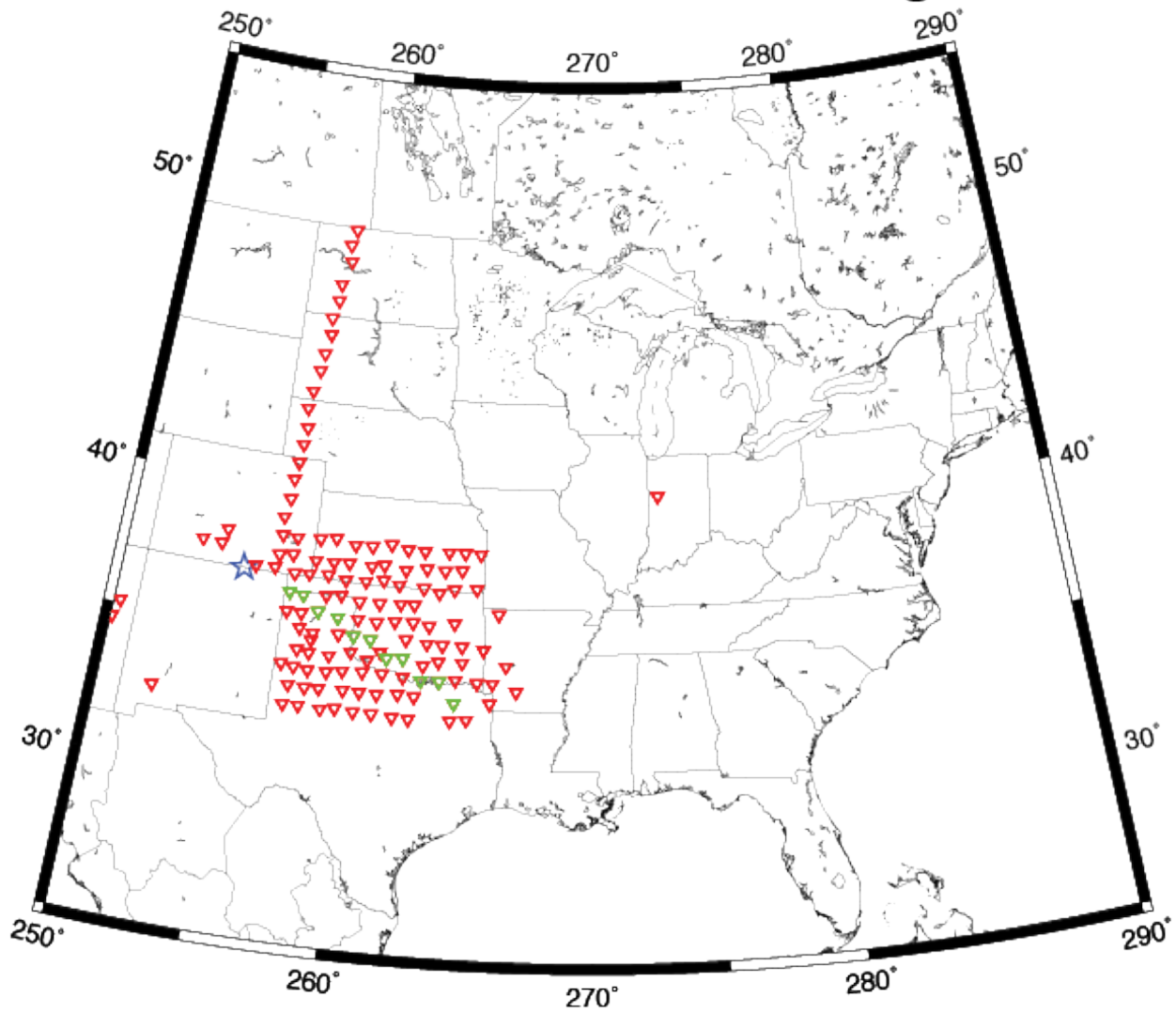


Figure 20: Map of epicenter (blue star) and stations examined (inverted triangles) for the 2010 $M3.6$ southern Colorado earthquake. Green stations form the southeast profile through Oklahoma.

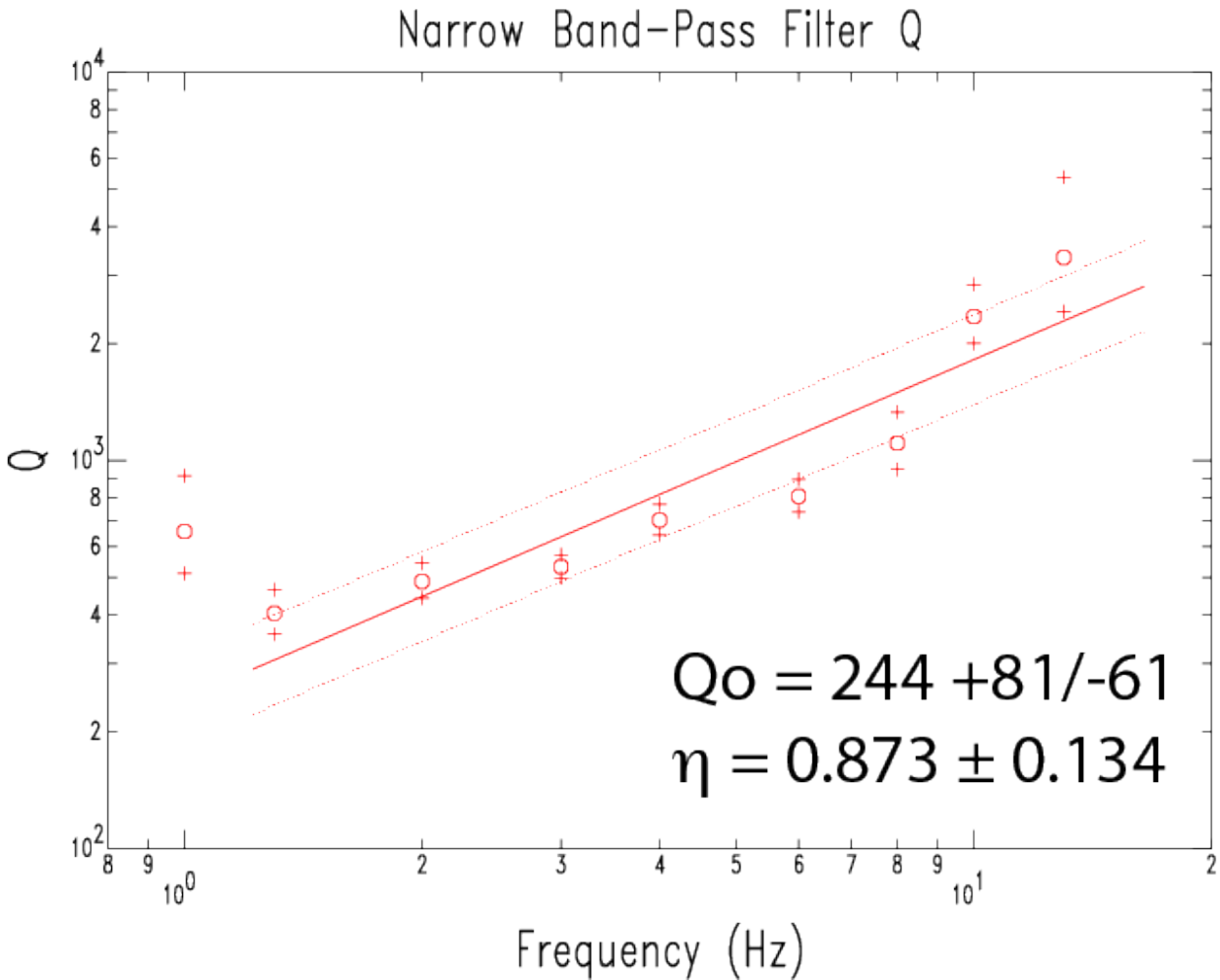


Figure 21: Individual earthquake $Q(f)$ plot for the green profile in Figure 20. Lines and symbols have the same meaning as in Figures 13 and 15.

Gulf Coast GMPE

Whole record spectral amplitudes were used in the Gulf Coast GMPE development. At short periods (less than 3 s) the amplitudes are dominated by S and Lg amplitudes. At longer periods (greater than 3s) many records have strong surface waves, which can dominate the amplitudes at these periods. Surface waves in the Gulf Coast thick sediments are common and are important to the ground motion amplitudes expected at sites in the Gulf Coast.

Focal mechanisms were not available for the smaller earthquakes (less than M4) in the Gulf Coast ground motion database. There are only records from 11 earthquakes in the database. So as not to spread these few events over three focal mechanism categories in the Gulf Coast GMPE development, we have not included focal mechanism terms (a_2*RR and a_3*SS) in the final set of coefficients for our GMPE relation shown in Equation 6. Coefficient a_1 and the uncertainty terms provided are applicable for all focal mechanisms in the Gulf Coast region.

Figure 22 presents the magnitude-distance distribution of the 549 records in the Gulf Coast ground motion database. There are some observations, although limited, at distances less than 100 km where geometrical spreading is important. Most of this close-in data comes from the **M**7.1 2010 Darfield, NZ earthquake. We have used a linear geometrical spreading term over all distances because the data is not sufficient to properly define a bilinear or trilinear form that might be expected in the region.

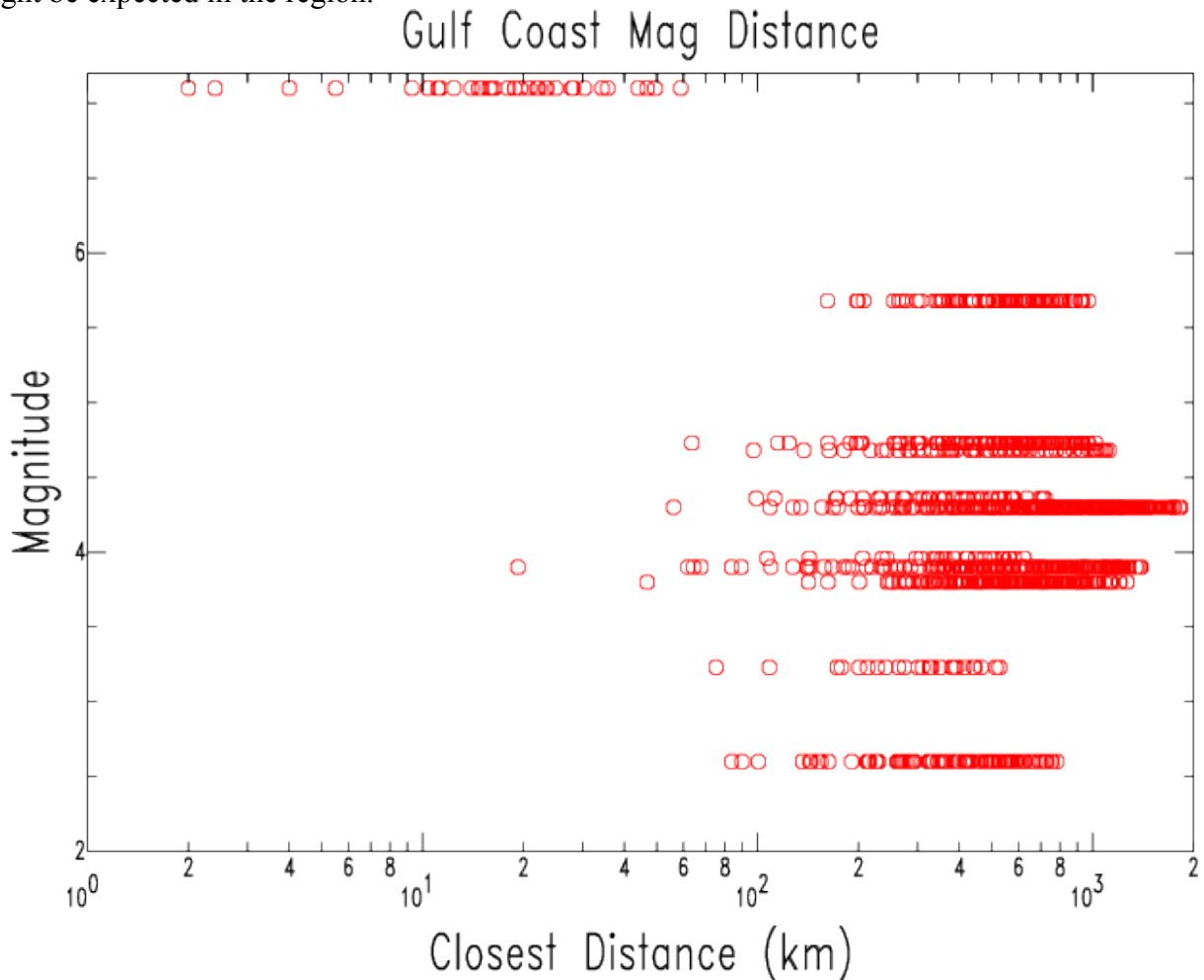


Figure 22: Magnitude-distance distribution for the Gulf Coast *Q* region dataset of this study.

As to estimates of V_{s30} at the recording sites, the thick sediments of the Gulf Coast region limited the range of assigned V_{s30} values to 140 – 1300 m/s. Most of the V_{s30} values are less than 600 m/s.

Brune stress drop estimates for these events range from 3 to 10 MPa. These values are typical of natural and potentially induced earthquakes in the Gulf Coast and southern central US (Cramer, 2016). However, the 2010 **M**3.9 South Texas earthquake has a very low Brune stress drop of 0.3 MPa. And the 2012 **M**2.6 Alabama Coast earthquake had an even lower stress drop of 0.02 MPa. These very low Brune stress drops are due to the earthquakes occurring in the very thick Gulf Coast unconsolidated sediments.

Table 6 provides the regression results at 23 periods: PGA, PGV, and 0.1, 0.2, 0.3, 0.4, 0.5, 0.6, 0.7, 0.75, 0.8, 0.9, 1.0, 2.0, 3.0, 4.0, 5.0, 6.0, 7.0, 7.5, 8.0, 9.0, and 10.0 s.

Table 6: Regression coefficients for rupture (closest) distance.

GULF Coast GMPE Coefficients (Rupture Distance)

Period	a ₁	b ₁	b ₂	c ₁	c ₂	c ₃	d ₁	φ	τ _u	σ _{TU}
PGA	-3.8777	1.2637	-0.0919	-1.9436	0.1572	-0.0017	-0.0802	0.22	0.33	0.40
PGV	-0.8283	0.8188	-0.0449	-2.5653	0.2310	-0.0006	-0.4062	0.46	0.66	0.80
0.1	-2.2456	0.8622	-0.0626	-2.1799	0.1961	-0.0020	0.0685	0.25	0.39	0.46
0.2	-5.6733	1.6471	-0.1022	-0.9549	0.0173	-0.0024	-0.0304	0.26	0.39	0.47
0.3	-5.5372	1.5225	-0.0914	-1.0053	0.0405	-0.0023	-0.1878	0.23	0.37	0.44
0.4	-5.7131	1.5369	-0.0936	-1.0527	0.0554	-0.0021	-0.3088	0.23	0.34	0.41
0.5	-5.6452	1.5148	-0.0919	-1.1825	0.0659	-0.0019	-0.3570	0.22	0.31	0.38
0.6	-5.4355	1.4323	-0.0864	-1.3227	0.0910	-0.0017	-0.3561	0.21	0.27	0.34
0.7	-5.3608	1.4065	-0.0861	-1.4689	0.1149	-0.0015	-0.4004	0.21	0.24	0.32
0.75	-5.4487	1.4416	-0.0886	-1.4836	0.1112	-0.0015	-0.4216	0.20	0.23	0.31
0.8	-5.6302	1.4944	-0.0925	-1.4562	0.1034	-0.0014	-0.4415	0.21	0.22	0.30
0.9	-5.7389	1.5680	-0.1010	-1.5518	0.1097	-0.0012	-0.4571	0.20	0.22	0.30
1.0	-5.6125	1.5366	-0.0984	-1.6437	0.1143	-0.0010	-0.4646	0.20	0.22	0.30
2.0	-8.0066	2.4562	-0.1853	-2.0961	0.1597	-0.0003	-0.7207	0.23	0.24	0.33
3.0	-7.6956	2.2222	-0.1625	-2.2426	0.1919	-0.0002	-0.6639	0.22	0.29	0.36
4.0	-8.5263	2.3783	-0.1648	-1.9675	0.1305	-0.0003	-0.5852	0.24	0.30	0.38
5.0	-8.8509	2.3787	-0.1558	-1.8273	0.0921	-0.0001	-0.5973	0.24	0.35	0.43
6.0	-7.9916	2.0065	-0.1229	-1.8918	0.1052	0.0000	-0.6491	0.26	0.36	0.45
7.0	-7.9137	1.8841	-0.1108	-1.9341	0.1196	0.0001	-0.6893	0.27	0.37	0.46
7.5	-8.4775	2.0289	-0.1211	-1.8662	0.1097	0.0000	-0.6996	0.27	0.38	0.46
8.0	-8.7210	2.1075	-0.1288	-1.9113	0.1176	0.0001	-0.6969	0.27	0.39	0.47
9.0	-8.5466	2.0336	-0.1266	-2.0998	0.1557	0.0001	-0.7058	0.27	0.39	0.48
10.0	-8.1012	1.8856	-0.1185	-2.3024	0.1920	0.0002	-0.6768	0.26	0.39	0.47

$$\log Y = a_1 + b_1 M + b_2 M^2 + (c_1 + c_2 M) \log R + c_3 (R - R_0) + d_1 \log \frac{V_s}{V_{ref}}$$

Figure 23-27 present comparisons to observations used in the regression at selected periods and five magnitudes. The comparison periods are PGA, PGV, 0.2 s, and 1.0 s for moment magnitudes 7.1, 5.7, 4.7, 4.3, and 3.9. Only observations from earthquakes with magnitudes near the regression curves are shown. The regressions follow the data well, except for PGV which has some added variability to the left and right of the fit. Generally, the datasets from different earthquakes overlap. At M4.7 (Figure 25) at PGV and 1.0 s there is some separation in the observations from the Prague OK foreshock and the Greenbrier AR mainshock, although they agree well at short periods. A greater separation occurs between the Arcadia OK and South Texas earthquakes at short periods (Figure 27), but not at long periods. The South Texas earthquake is located in southern Texas near the coast of the Gulf of Mexico (Figure 8) where the sediment thickness exceeds 10 km, unlike the other events, including the Alabama coast earthquake, where sediment thickness is less than 10 km. The observed Brune stress drop for the South Texas earthquake is very low at 0.3 MPa instead of the usual value of 5-10 MPa. The observed reduced amplitudes at short periods for the South Texas earthquake are likely related to the very low stress drop for that earthquake. The stress drop reflects the earthquake occurring at shallow depths in very thick sediments. The regression tends to follow the Arcadia OK data

indicating that at short periods the other earthquakes in the dataset with 5-10 MPa Brune stress drops are controlling the fit to observations more than the data from the South Texas earthquake.

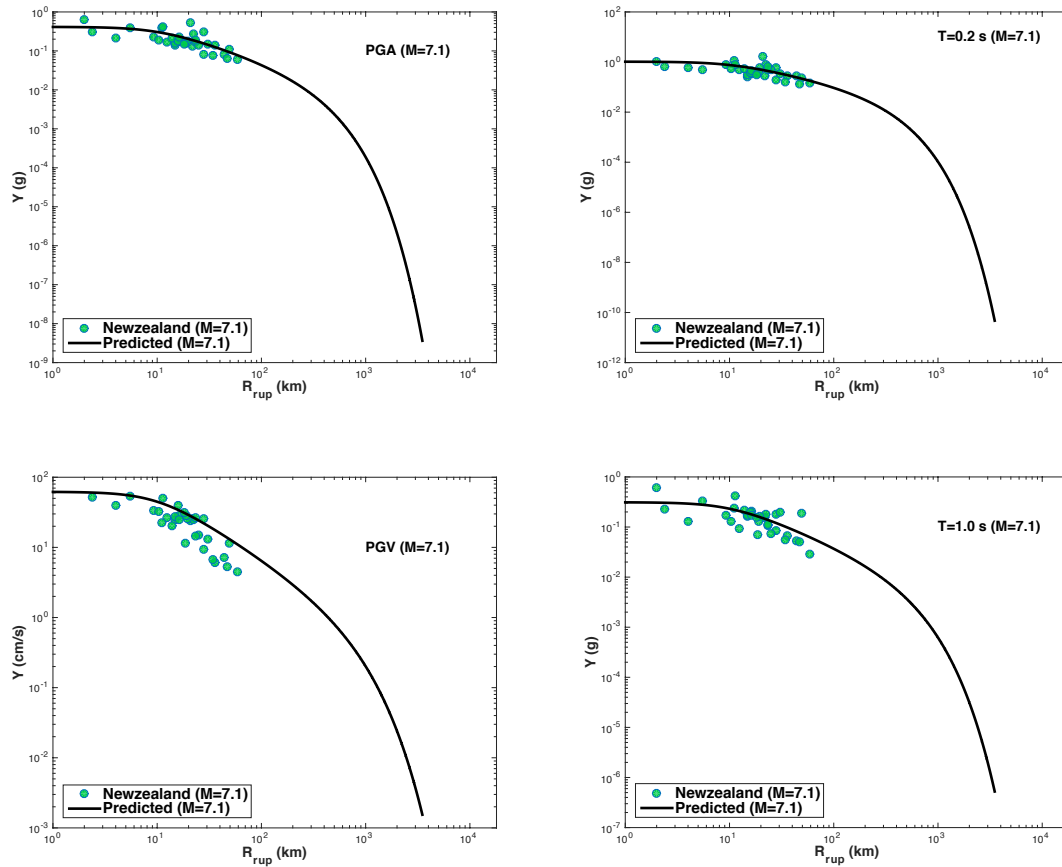


Figure 23: Comparison of regressions and observations for $M7.1$ at PGA (top left), PGV (bottom left), 0.2 s (top right), and 1.0 s (bottom right).

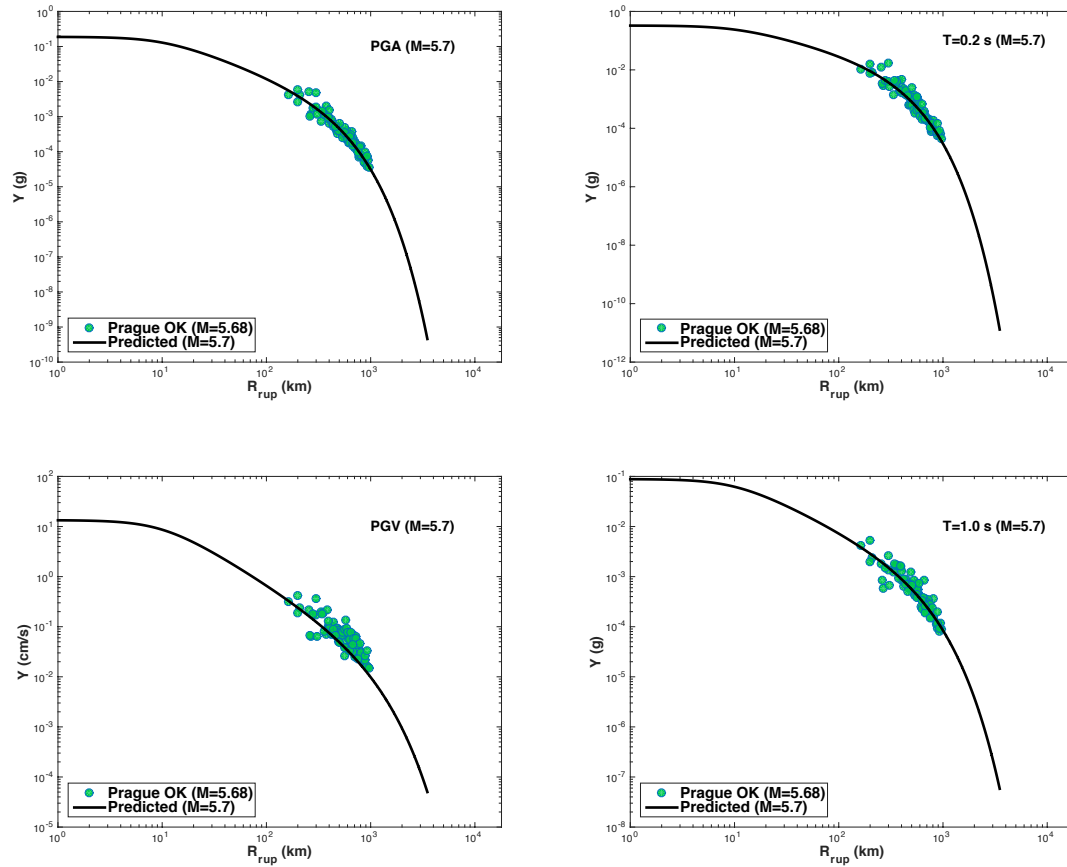


Figure 24: Comparison of regressions and observations for $M5.7$ at PGA (top left), PGV (bottom left), 0.2 s (top right), and 1.0 s (bottom right).

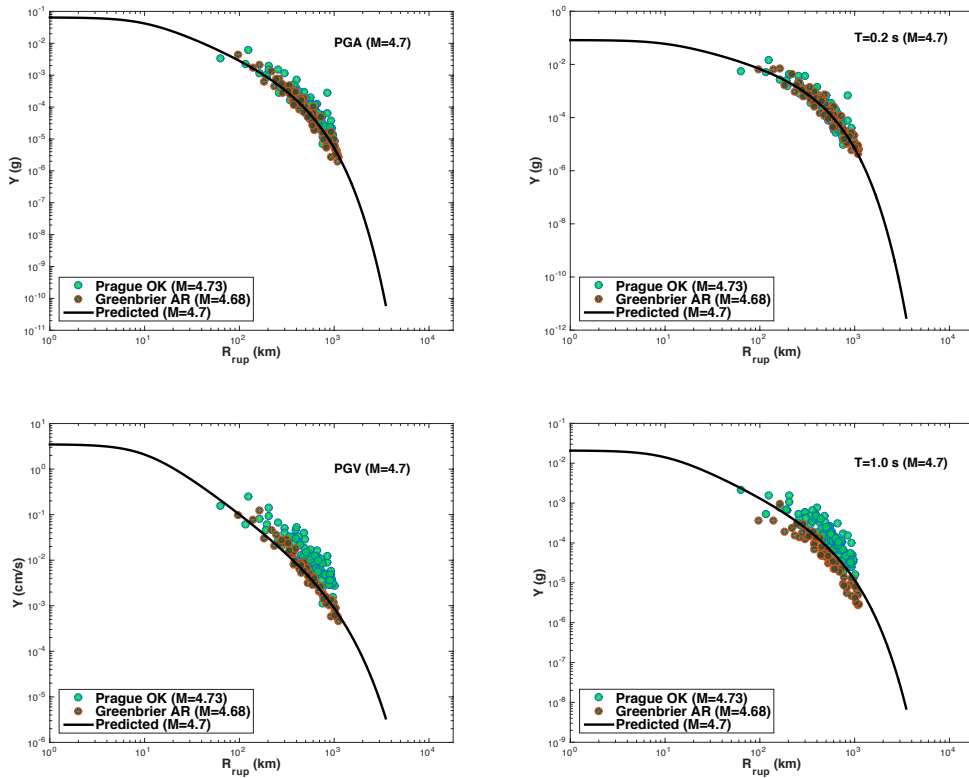


Figure 25: Comparison of regressions and observations for $M4.7$ at PGA (top left), PGV (bottom left), 0.2 s (top right), and 1.0 s (bottom right).

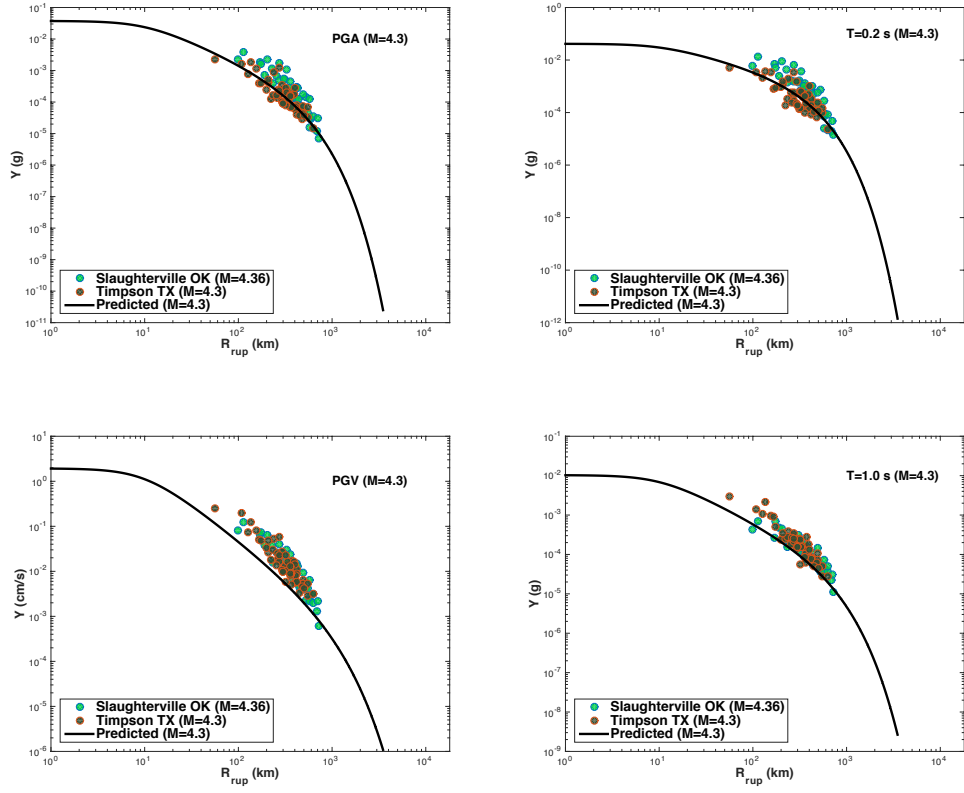


Figure 26: Comparison of regressions and observations for $M4.3$ at PGA (top left), PGV (bottom left), 0.2 s (top right), and 1.0 s (bottom right).

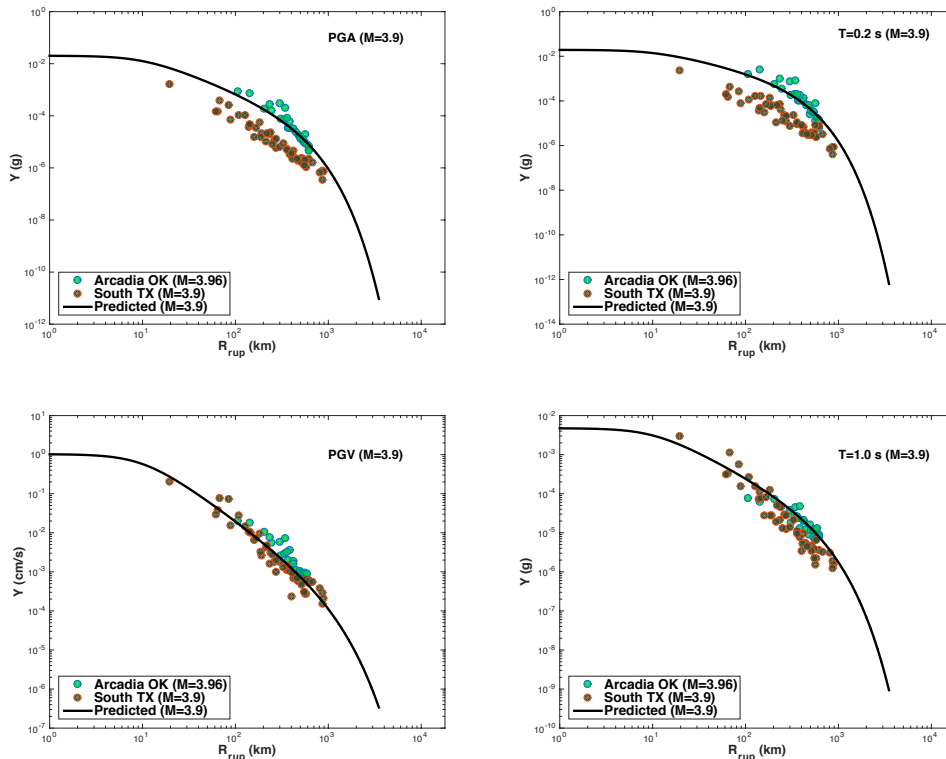


Figure 27: Comparison of regressions and observations for $M_{3.9}$ at PGA (top left), PGV (bottom left), 0.2 s (top right), and 1.0 s (bottom right).

Aleatory variability from the regression is presented in Figure 28. Usually, between event sigma is less than within event sigma in a regression with lots of events and observations (for example see Al Noman and Cramer, 2015, Figure 8.7). However, for our Gulf Coast GMPE this relationship is reversed, possibly due to the limited number of earthquakes available. While the variability is typical for most periods (total sigma 0.3 to 0.5), the variability is unusually large for PGV (period of -0.1, total sigma 0.80) due to the increased variability to the left and right of the fit curve noted above in Figures 23 through 27. Possibly this is related to the geologic setting and limited observations and/or to the form of our regression.

Scaling

Scaling with V_{s30} , magnitude, and distance for all 23 periods is presented in Figures 29 – 32. The line color and type are common to these four figures. The V_{s30} scaling is atypical at short periods (PGA, 0.1-0.3 s) (for example see Al Noman and Cramer, 2015, Figure 8.8 as a comparison). Likely this is due to the geologic setting in the Gulf Coast and most of the V_{s30} values being less than 600 m/s. The magnitude and distance scaling is more typical, although at a slightly lower ground motion level (compare with Al Noman and Cramer, 2015, Figures 8.9-8.11). As expected due to lower Q , the predicted ground motions are significantly lower at large distances than predictions from mid-continental CEUS relations.

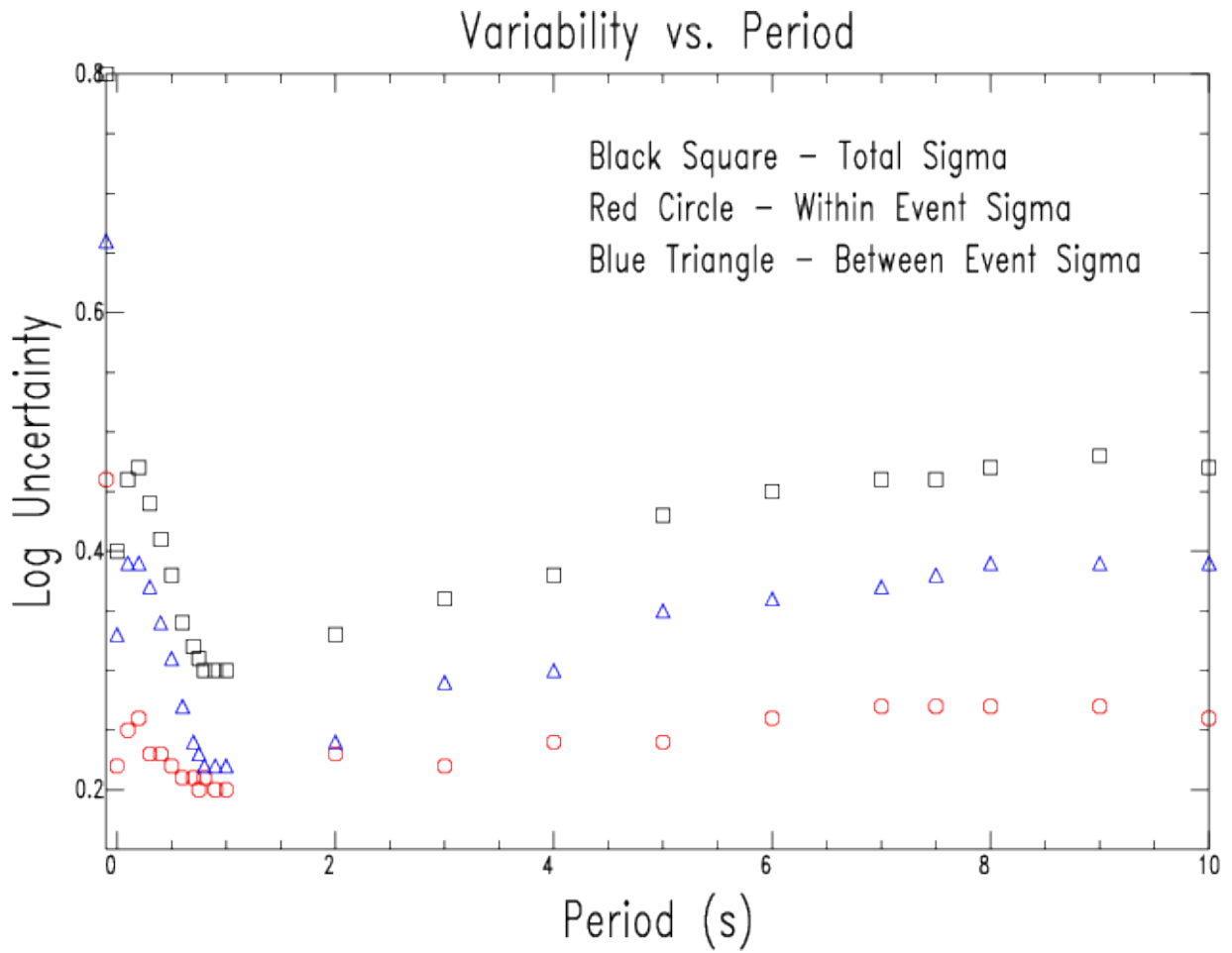


Figure 28: Regression aleatory variability as a function of period. A period of -0.1 represents PGV and a period of 0.0 represents PGA.

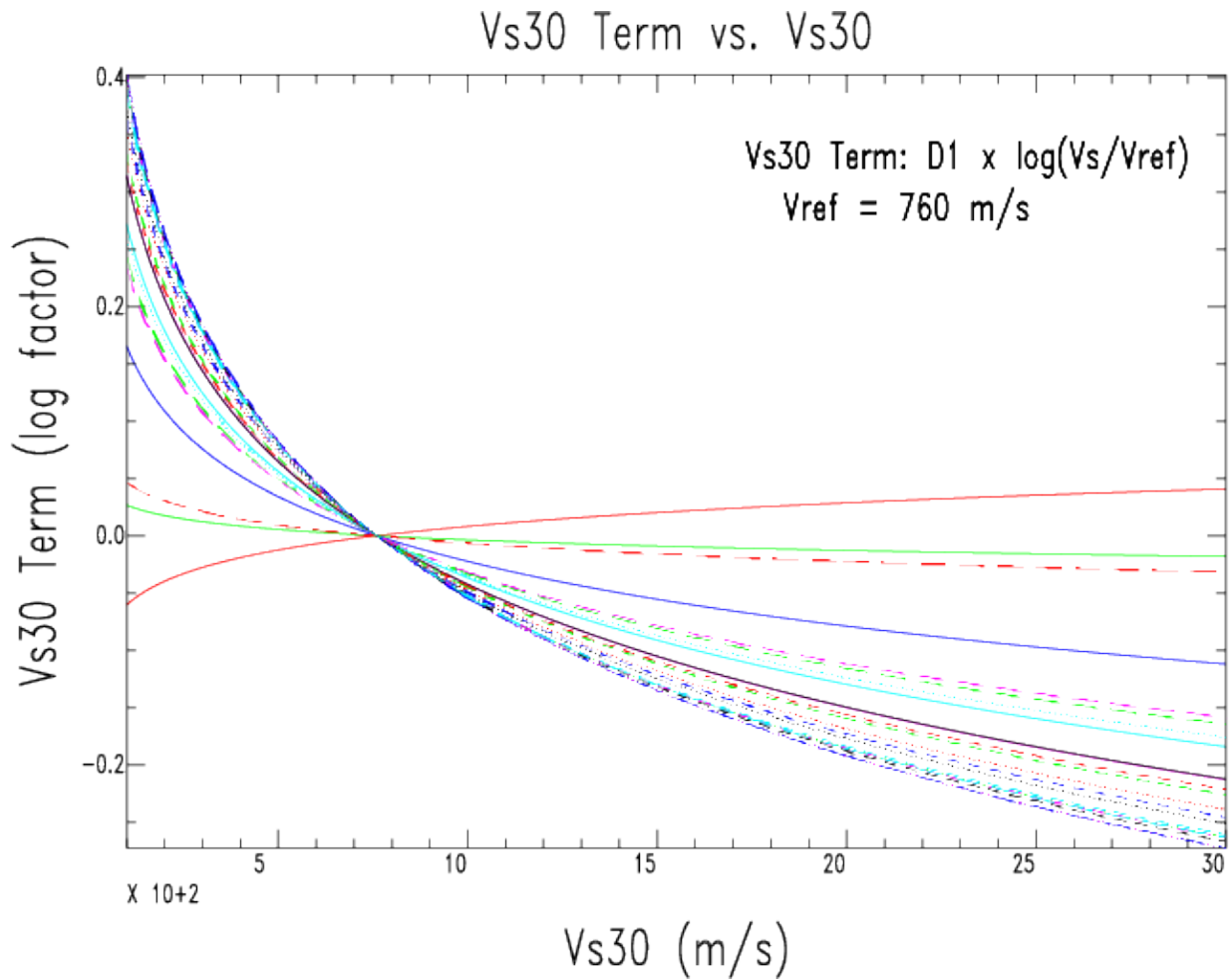


Figure 29: Vs30 scaling for all 23 periods. Solid lines: red – 0.1s, green – 0.2s, blue – 0.3s, cyan – 0.4s, magenta – 0.5s, and black – 0.6s. Dotted lines: red – 0.7s, green – 0.8s, blue – 0.9s, cyan – 1.0s, magenta – 2.0s, and black – 3.0s. Short dashed lines: red – 4.0s, green – 5.0s, blue – 6.0s, cyan – 7.0s, magenta – 8.0s, and black – 9.0s. Long dashed lines: red – PGA, green – 0.75s, blue – 7.5s, cyan – 10.0s, magenta - PGV.

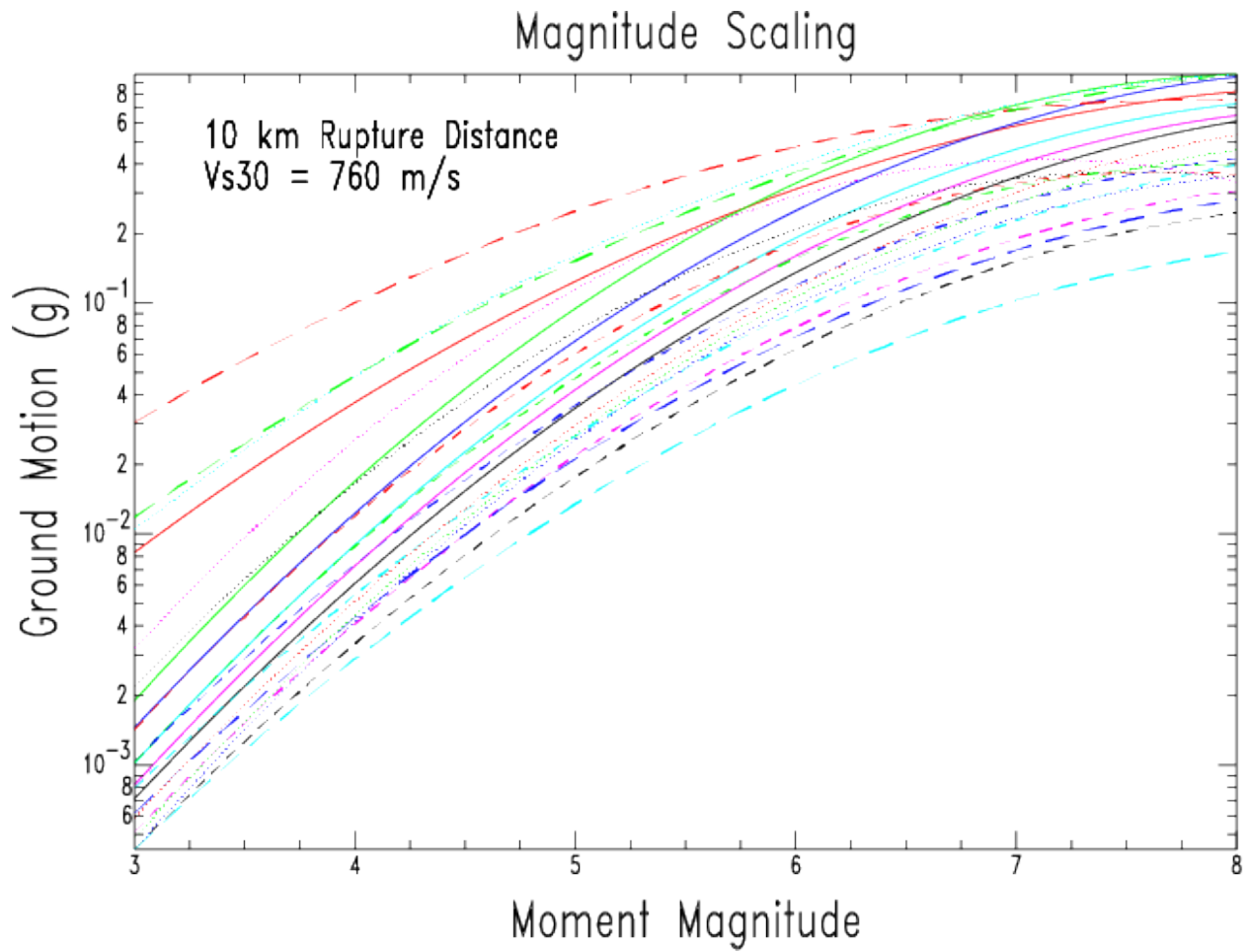


Figure 30: Magnitude scaling for 22 periods. Period representation by line color and type is the same as Figure 29, except PGV is not shown due to different units and scale.

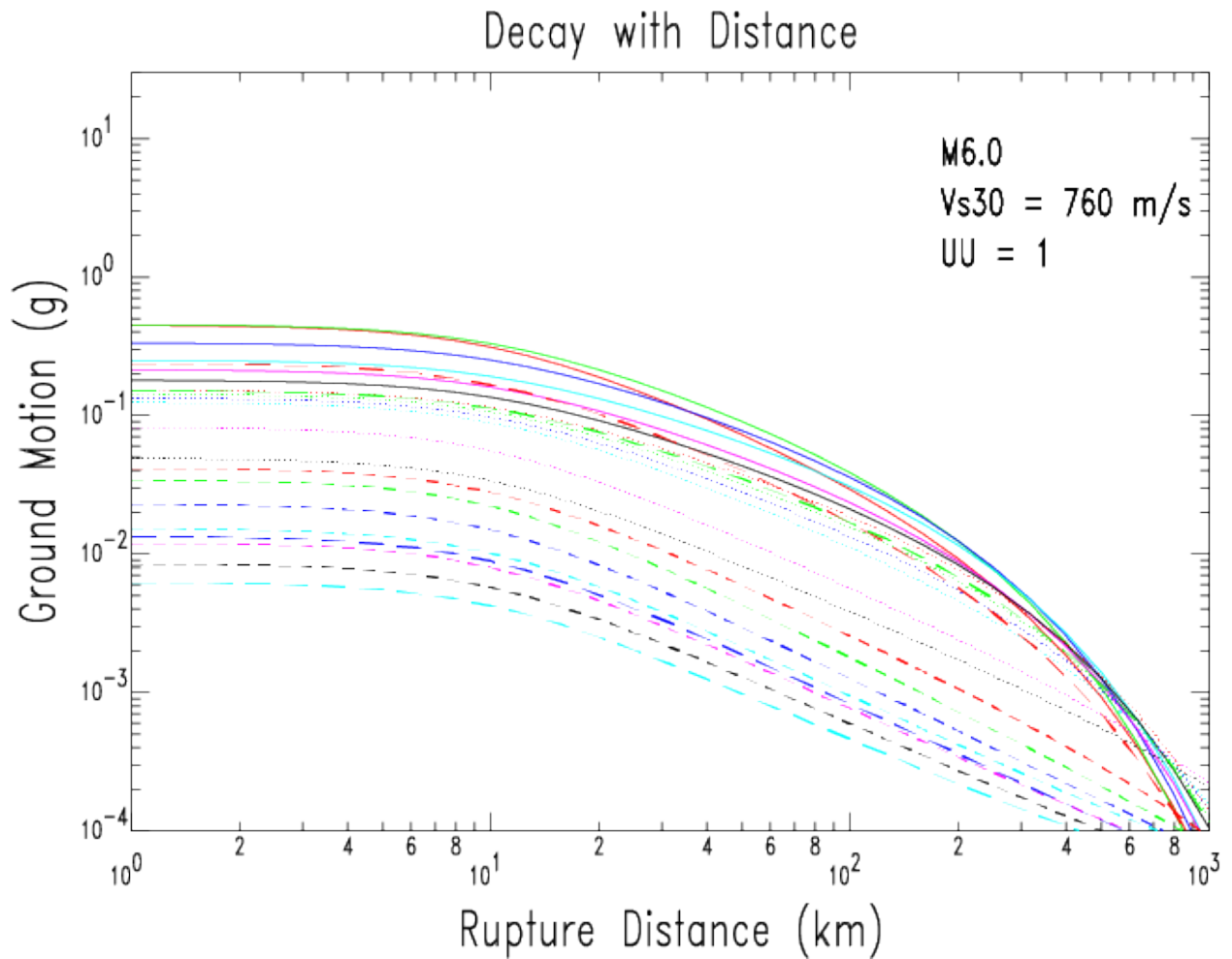


Figure 31: Predicted decay with distance at 22 periods at M6.0. Period representation by line color and type is the same as Figure 29, except PGV is not shown due to different units and scale.

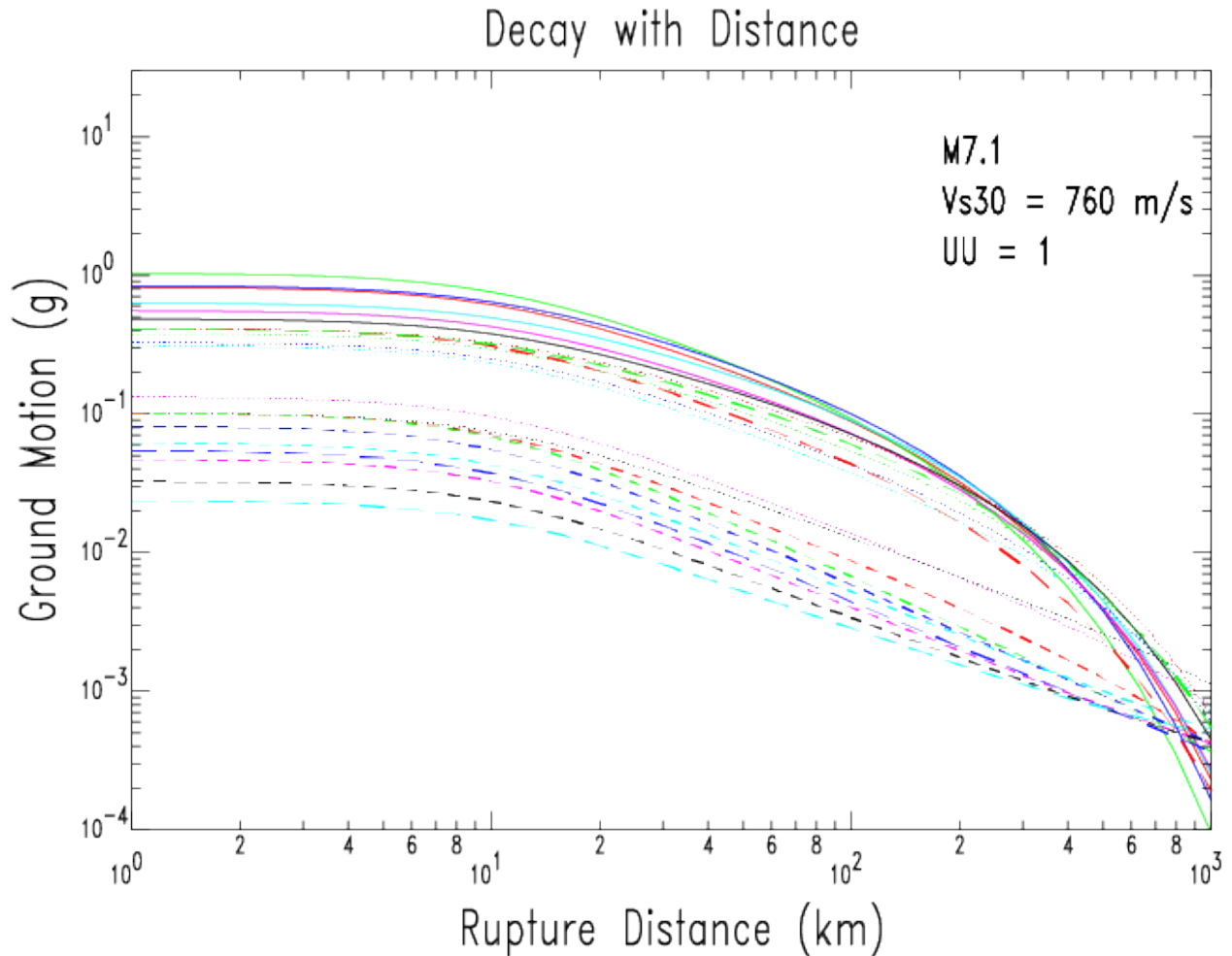


Figure 32: Predicted decay with distance at 22 periods at M7.6. Period representation by line color and type is the same as Figure 29, except PGV is not shown due to different units and scale.

Ground motion saturation is demonstrated in Figure 33 with stronger saturation at short periods than at long periods. Also at short periods, saturation is obviously a function of magnitude and distance, while at long periods it is more dominantly a function of just magnitude. Additionally, at long periods Gulf Coast decay with distance is slower, particularly at large magnitudes, possibly due to the geologic setting and the more likely presence of surface waves.

Comparison to other GMPEs

The two other published Gulf Coast GMPEs are Toro et al. (1997) and Silva et al. (2003). We compare our GMPEs to these two GMPEs in Figures 34 and 35. Generally, our GMPEs tend to compare well with the other GMPEs, but predict lower ground motions at distances less than 100 km. This may be due to our functional form using a simple linear geometrical spreading term and the lack of observations for distances less than 50 km. At short periods our GMPEs tend to higher attenuation beyond 500 km due to the observed lower Gulf Coast Q than previously published.

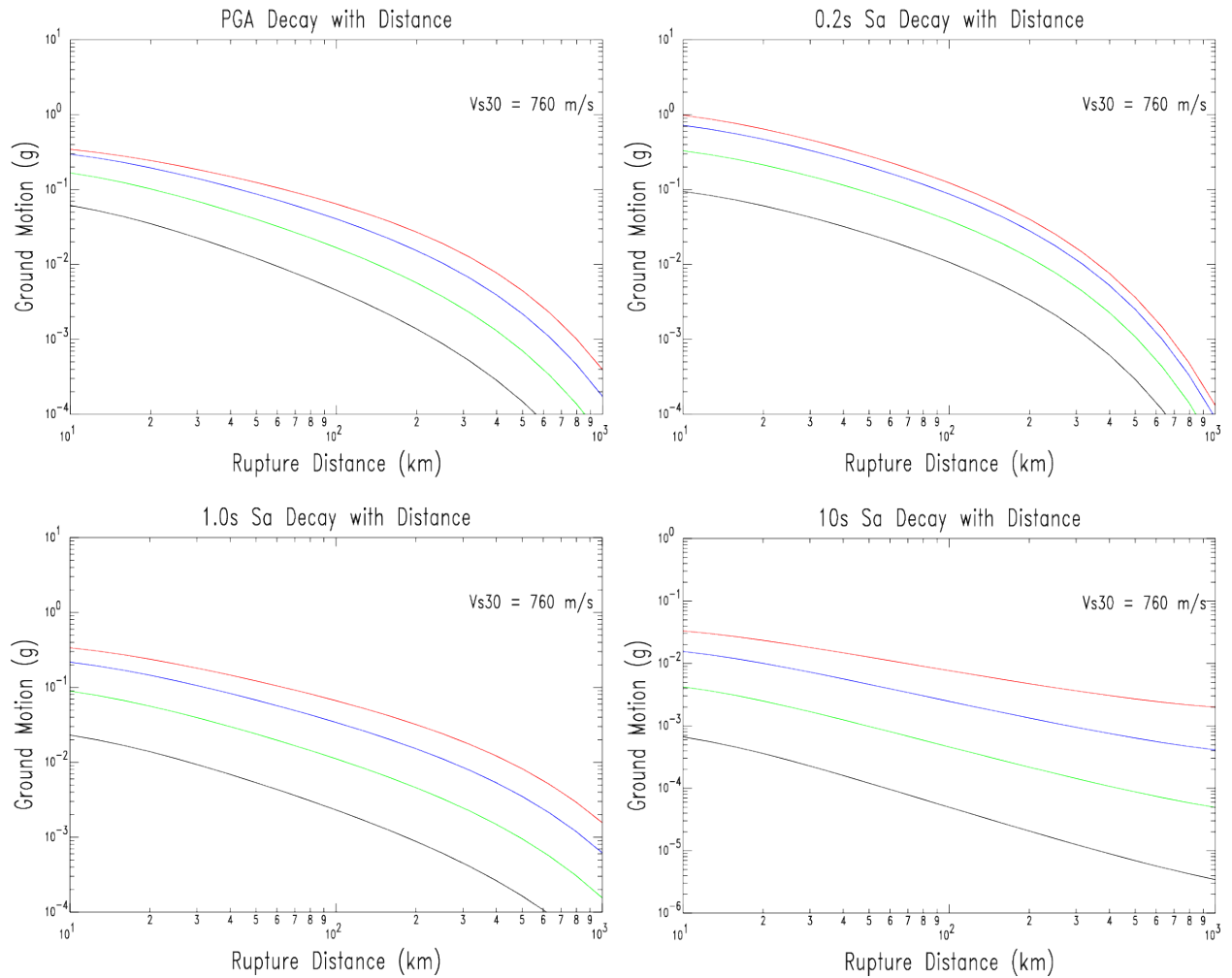


Figure 33: Ground motion saturation for PGA (upper left), 0.2 s (upper right), 1.0 s (lower left), and 10.0 s (lower right). Decay with distance is shown for M8.0 (red), M7.0 (blue), M6.0 (green), and M5.0 (black).

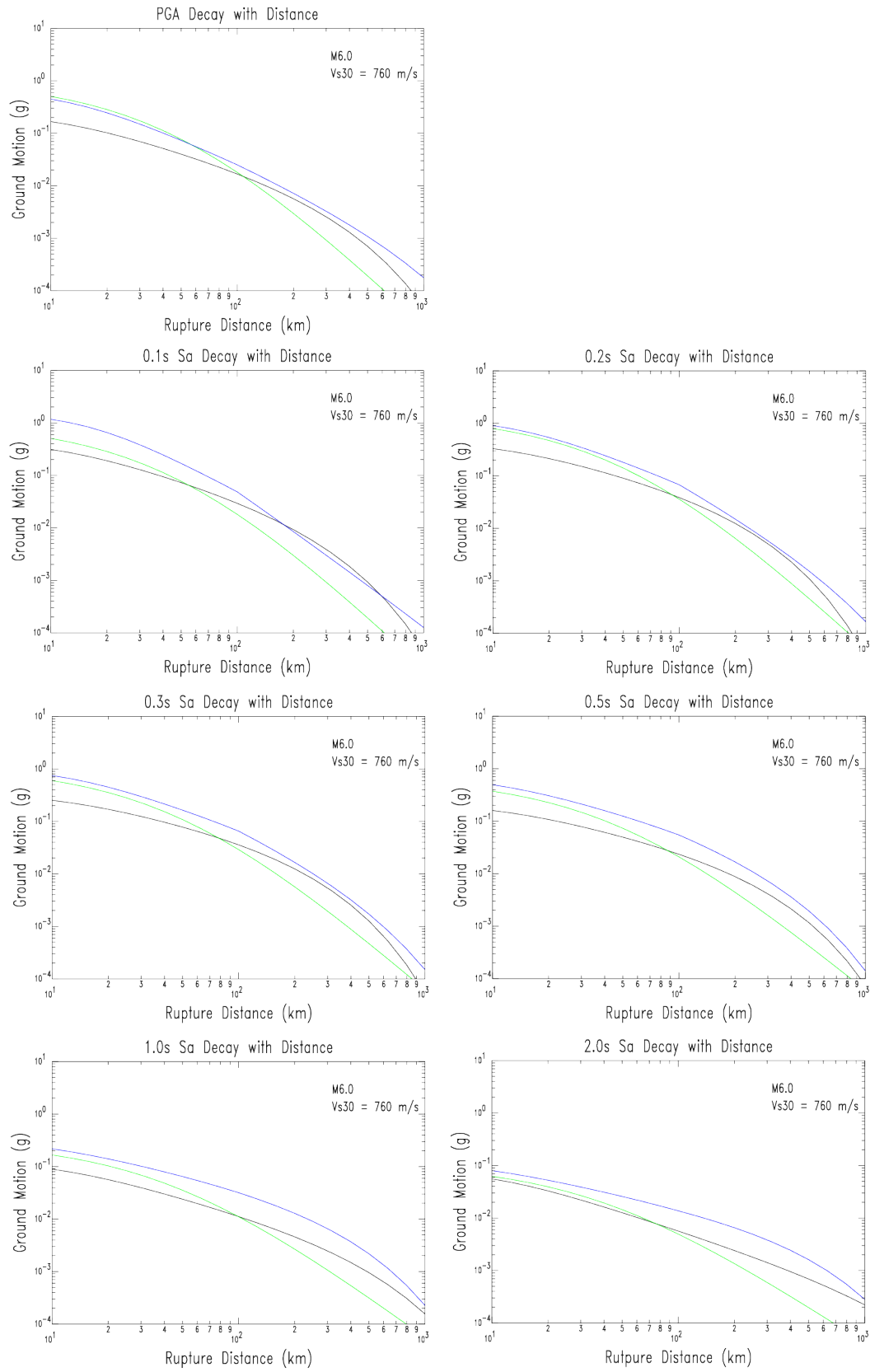


Figure 34: Comparison for $M6.0$ and selected periods of our GMPE (solid black) with two other Gulf Coast GMPEs (colored).

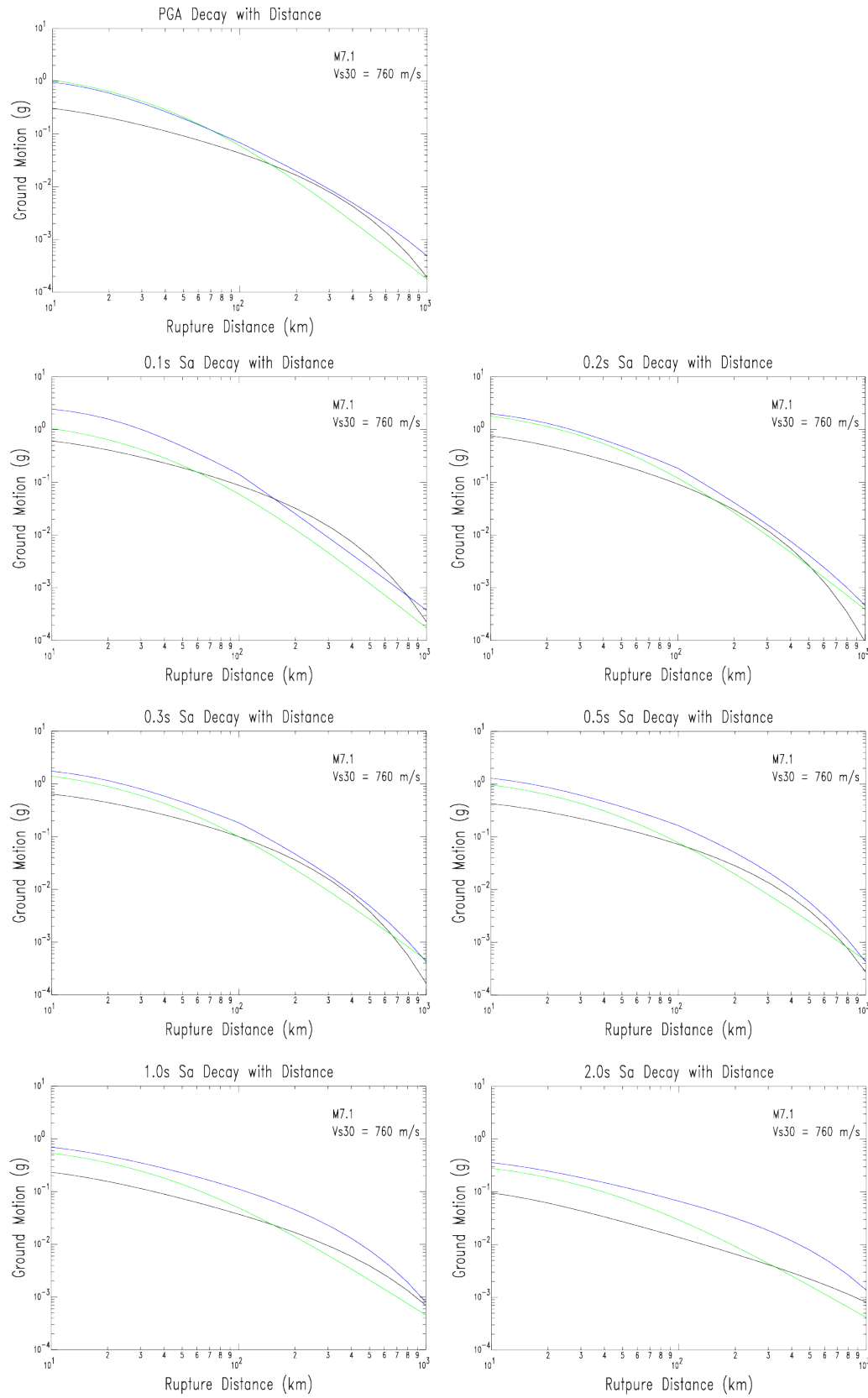


Figure 35: Comparison for M7.1 and selected periods of our GMPE (solid black) with two other Gulf Coast GMPEs (colored).

Discussion

Gallegos et al. (2014) conducted a Q tomography study and published a Q_0 (Q at 1.0 Hz) map for the CEUS. Our 1 Hz Q boundary location from earthquakes outside the Gulf Coast region corresponds well with and confirms the Gallegos et al. results. However, our short period (5 Hz) results show high attenuation over a larger Gulf Coast region than the Gallegos et al. results at 1 Hz. Residual maps of log amplitude differenced with expected log amplitude relative to a reference profile (decay with distance) in the mid-continent Q region (see Figure 4) show radiation pattern and propagation effects that could complicate tomographic interpretations at short and long periods when too few observations (crossing raypaths) are available such as in the case of the Gallegos et al. (2014) study.

Our Q boundary study puts the transition near 34°N south of Memphis, TN for the northern Mississippi embayment. Our Gulf Coast $Q_0 = 259 +24/-22$ and $\eta = 0.715 \pm 0.013$ over a broad frequency band of 0.1 to 16 Hz applies to the region south of 34°N. The results of Zandieh and Pezeshk (2010) and Sedeghati and Pezeshk (2016) for intrinsic Q and coda Q (respectively) show a higher, mid-continent Q for New Madrid seismic zone observations north of 35°N, which is compatible with our observations. These Q results for the northern Mississippi embayment are somewhat similar to the regionalization of EPRI (1993) but contrary to the regionalization results from NGA East (Dreiling et al., 2014). Our, the Zandieh and Pezeshk (2010), and the Sedeghati and Pezeshk (2016) results are based on Q observations and not other regionalization parameters (seismotectonics or crustal velocity structure) with few Q observations.

The Gulf Coast Q study of Chapman and Conn (2016) covers a larger region than the Gulf Coast region defined in this study. Because the Chapman and Conn study includes regions with mid-continent Q around the margins of our Gulf Coast region, it is not surprising that Chapman and Conn estimate a higher Gulf Coast Q_0 (less attenuation) than we do. We believe we have properly defined the boundary of the high attenuating Gulf Coast region, so our Gulf Coast estimates of Q should be more accurate.

Our estimate of Gulf Coast regional Q(f) of $Q_0 = 259 +24/-22$ and $\eta = 0.715 \pm 0.013$ over a broad frequency band of 0.1 to 16 Hz using the approach of MacNamara (1996) is our best estimate of Q in the Gulf Coast region defined in this study. Individual earthquake dataset estimates of Q within the Gulf Coast region can show lower Q, particularly in the eastern portion of the Gulf Coast region (see Table 2). But the MacNamara approach allows for station and event terms in the Q inversion at a given period. Thus the MacNamara based results better allow for the observed thickening of the Gulf Coast sediments to the south as indicated by the station terms in Figure 11.

Our Gulf Coast GMPE is based on observed Q boundary locations and ground motions from raypaths entirely within the Gulf Coast region. Our Gulf Coast GMPE shows higher attenuation beyond 500 km than the previously published two Gulf Coast GMPEs. Because the thick sediments of the Gulf Coast tend to generate surface waves for earthquakes within the region, our whole record GMPE should allow for the larger surface wave ground motions at longer periods.

Strong regional Q variations in the southern CEUS can affect not only ground motion observations but also intensity observations in the same region. Hough's (2014) interpretation of potentially induced CEUS earthquakes having significantly lower (0.4 or greater magnitude units) intensity estimated magnitudes (M_{IE}) than moment magnitudes assumes that regional Q variations do not affect the intensity values in higher attenuating regions. The M_{IE} is determined by comparing the intensity decay with distance to the CEUS intensity relations of Atkinson and Wald (2007). The Atkinson and Wald (2007) relations are for mid-continental Q. Most of Hough's (2014) potentially induced earthquakes are in Colorado, Arkansas, Oklahoma, and Texas and have M_{IE} values ranging 0.6 to 1.3 magnitude units lower than M . These potentially induced earthquakes are located in regions of lower Q (higher attenuation). The one induced earthquake in the mid-continental Q region in Ohio has a 0.4 magnitude unit lower M_{IE} , while Hough's tectonic CEUS earthquakes have 0.0 to 0.2 magnitude unit lower M_{IE} . The Brune stress drop estimates in this report and from Cramer (2016) clearly show that potentially induced earthquakes do not have stress drops that differ significantly from shallow natural earthquakes, including the Ohio earthquake which has a Brune stress drop of 5 MPa (Cramer, 2016). This suggests earthquake M_{IE} values are correlated with regional Q, with the potentially induced earthquakes possibly having a remaining M_{IE} reduction of about 0.2 magnitude units that are not correlated with Q. This small reduction is not related to stress drop.

Further evidence that intensities are biased by regional Q is provided by Hough and Page (2015). Their assigned intensities for the 1952 $M5.7$ El Reno OK earthquake (their Figure S3a reproduced in Figure 36) show a distinct trend of extending to greater distances to the NE. From our results in Figure 7, azimuths to the NE from central Oklahoma are the only azimuths not affected by lower Q (higher attenuation) regions and basically representative of mid-continental Q. The same azimuthal dependence is shown in Hough and Page's Figure S3b (Figure 37 of this report) for intensities for the 2011 $M5.7$ Prague OK earthquake. Thus regional Q can affect intensities and hence the estimate of M_{IE} .

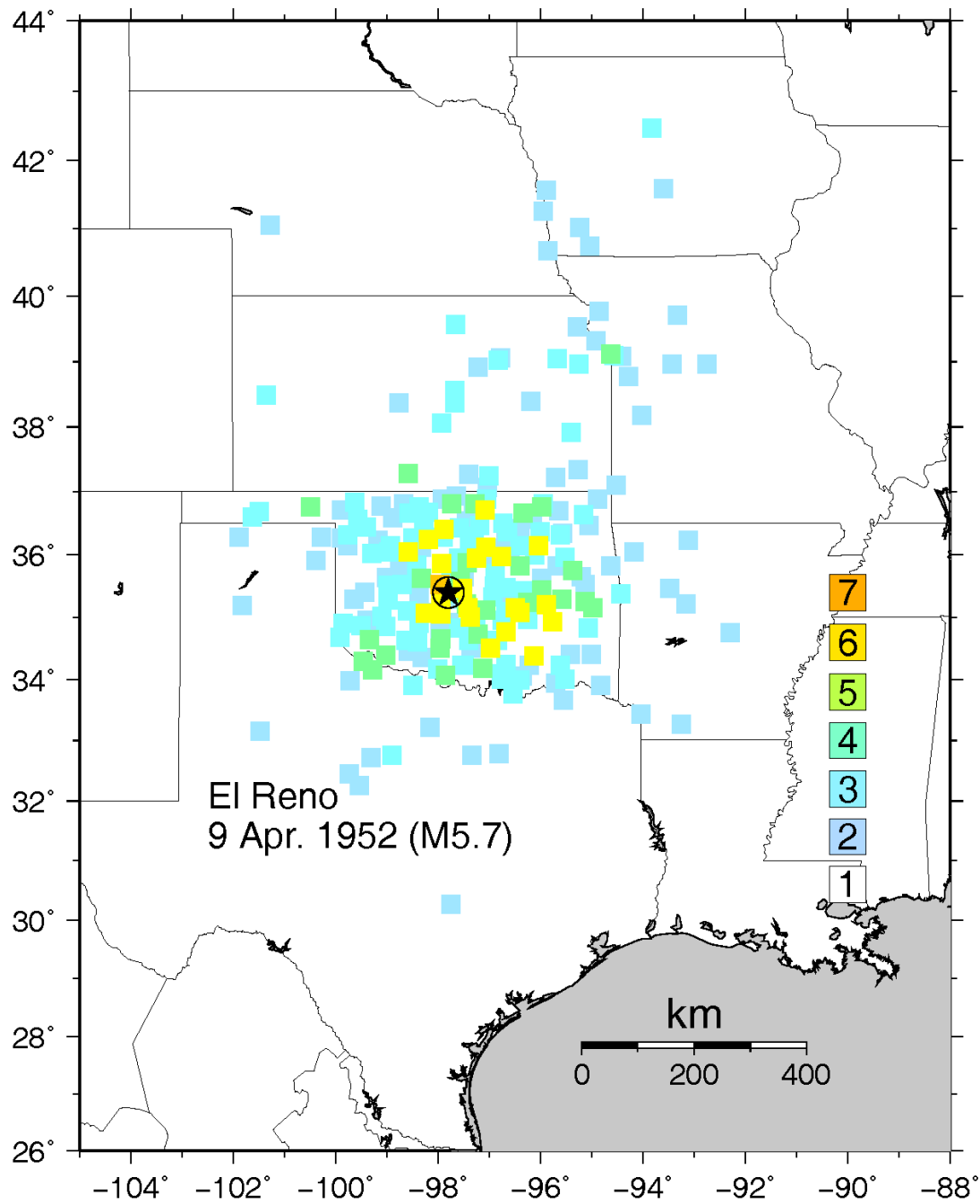


Figure 36: Intensities for the 1957 El Reno, OK M5.7 earthquake from Hough and Page, 2015.

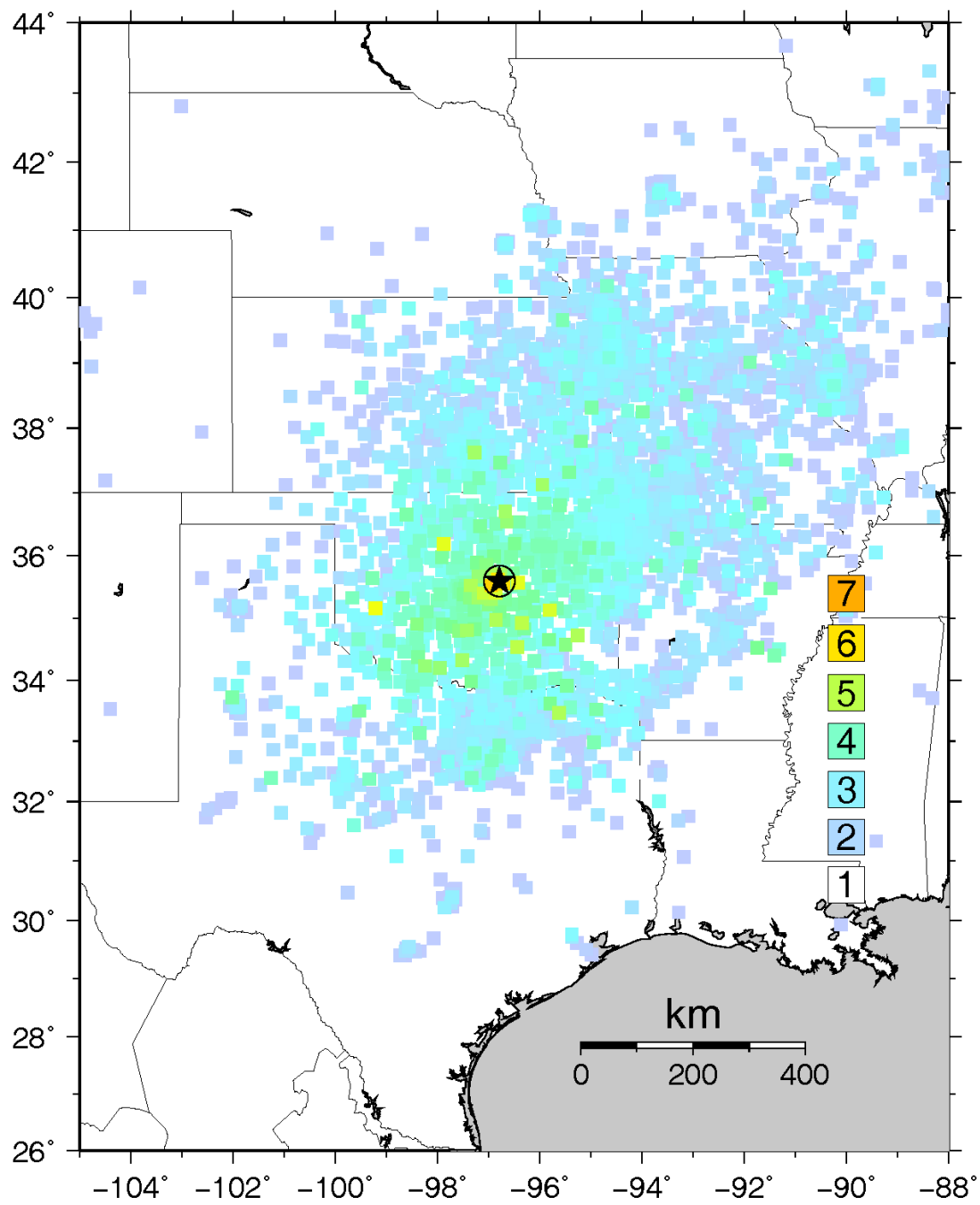


Figure 37: Intensities from the 2011 M5.6 Prague, OK earthquake from Hough and Page, 2015.

Summary

We have defined the location of the boundary between the low Q (higher attenuating) Gulf Coast and the high Q (lower attenuating) mid-continental regions in the CEUS from observations from the USArray. We show that the Gulf Coast Q region is different from the regionalizations from EPRI (1993) and NGA East (Dreiling et al., 2014), which had few Q observations available to them. The Florida peninsula and the Atlantic Coastal plain Q is similar to mid-continental Q and hence separate from the Gulf Coast Q region. Our Gulf Coast Q region roughly corresponds to the Ouachita thrust and/or the Alabama-Oklahoma transform shown by Thomas (2010) but extends into central Oklahoma. Our resolution of the boundary location is limited by the 70 km spacing of the USArray.

For earthquakes outside the Gulf Coast Q region, we observe that the long period (1 Hz) boundary is farther south than the short period (5 Hz) boundary location. Our 1 Hz boundary from outside earthquakes corresponds to and confirms the low 1 Hz Q region shown by Gallegos et al. (2014) from Q tomography. For earthquakes inside the Gulf Coast region, the Q boundary at both short and long periods corresponds and is similar to the short period boundary location for earthquakes outside the Gulf Coast region.

Regional $Q(f)$ has been estimated for both the Gulf Coast and Florida peninsula. Gulf Coast regional $Q(f)$ is Q_0 (Q at 1 Hz) = $259 +24/-22$ and $\eta = 0.715 \pm 0.013$ over a broad frequency band of 0.1 to 16 Hz. The Florida peninsula Q is similar to mid-continental Q_0 but with a low η , suggesting a constant Q of about 1000. As previously published by others, our Atlantic Coastal Plain $Q(f)$ observations are similar to mid-continental Q. Our value of Gulf Coast $Q(f)$ is lower than that of Chapman and Conn (2016) because they averaged Q over a larger region that included portions of mid-continental Q crust, according to our study.

East of the Rocky Mountains and west of the Gulf Coast Q region are crustal basins and structures that can affect Q. In this study, we only have preliminary results for western Texas, western and central Oklahoma, and southern Kansas. They suggest that Q at long periods (1 Hz) is similar to mid-continental Q through out this region, but at short periods (5 Hz) it can be similar to Gulf Coast Q. The Southern Oklahoma Rift is a narrow E-W structure that connects to the Gulf Coast region and exhibits azimuthal dependent Q. E-W raypaths indicate Gulf Coast Q while N-S raypaths show Q that is between Gulf Coast and mid-continent Q. There is a suggestion of low 5 Hz Gulf Coast like Q in central Kansas, central Oklahoma, and western Texas, but not central Texas. Further work is needed to better define Q in these regions.

Based on the Gulf Coast Q boundary of this study, we have developed within Gulf Coast GMPEs for PGA, PGV, and 21 spectral acceleration (S_a) periods between 0.1 s and 10 s. We have used a dataset of 10 within Gulf Coast earthquakes and their recordings within the Gulf Coast for magnitudes ranging from M 2.6 to 5.7 and epicentral distances from 20 to 1000 km. Additionally, we used the 2010 M 7.1 Darfield, NZ observations for epicentral distances 8 to 70 km (rupture distances less than 60 km), which are unaffected by a regional Q_0 of about 100 and represent distances dominated by geometrical spreading. The Darfield observations provide some constraint at large magnitudes for which Gulf Coast observations are not available.

Intensity observations should be affected by regional Q just as ground motions are affected. We find support for this in the intensity observations of Hough and Page (2015) for the 1957 El Reno OK and 2011 Prague OK M5.7 earthquakes. The Hough and Page observations for these two earthquakes show less attenuation with distance (intensity values extending to greater distances) to the NW. This corresponds to the azimuth from central Oklahoma that shows dominantly mid-continental Q in our ground motion study, while other azimuths are affected by Gulf Coast like Q. This correlation of intensity decay with distance and regional Q is important to interpreting intensity from potentially induced earthquakes versus natural earthquakes in terms of source parameters such as stress drop. This is evident in the strong correlation of differences between earthquake M and M_{IE} (intensity estimated magnitude) in Hough (2014) with the regional Q affecting those earthquakes but not stress drop (see Discussion above).

Acknowledgements

Figures in the report were generated using SAC (Goldstein et al., 2003) and GMT (Wessel and Smith, 1991). CEUS earthquake data was downloaded from the IRIS DNC. The Darfield, NZ data was downloaded from fp.geonet.org.nz/strong/processed/Proc/09_Darfield_mainshock_extended_pass_band/Vol2/data (last accessed August 2, 2016).

References

- Al Noman, M.N. (2013). *Ground motion modeling for eastern North America: an empirical approach with the NGA-East database*, M.S. thesis, University of Memphis, Memphis, TN, 54 pp.
- Al Noman, M.N., DeShon, H.R., Cramer C.H. (2012), Ground motion prediction for ENA: learning from and limitations of the NGA-East database (abstract), Seismological Society of America Meeting-2012, San Diego, California, April. 2012, *Seism. Res. Lett.* **83**, 354.
- Al Noman, M.N., and C.H. Cramer (2015), Chapter 8: Empirical ground motion prediction equations for eastern North America, in *NGA East: Median Ground Motion Models for the Central and Eastern North America Region*, PEER Center Report 2015/04, Berkeley, California.
- Atkinson, G.M., and D.M. Boore (2014), The attenuation of Fourier amplitudes for rock sites in eastern North America, *Bull. Seism. Soc. Am.* **104**, 513-528.
- Atkinson, G.M., and R.F. Mereu (1992), The shape of ground motion attenuation curves in southeast Canada, *Bull. Seism. Soc. Am.* **82**, 2014-2031.
- Atkinson, G.M. and D.J. Wald (2007), "Did you feel it?" intensity data: A surprisingly good measure of earthquake ground motion, *Seism. Res. Ltr.* **78**, 362-368.

Benz, H.M., A. Frankel, and D.M. Boore (1997), Regional Lg Attenuation for the Continental United States, *Bull. Seis. Soc. Am.* **87**, 606-619.

Chapman, M., and A. Conn (2016), A model of Lg propagation in the Gulf Coast Plain of the southern United States, *Bull. Seism. Soc. Am.* **106**, 349-363.

Claerbout, J. F. (1976), *Fundamentals of geophysical data processing with applications to petroleum prospecting*, McGraw-Hill, New York, NY, 274 pp.

Cramer, C.H. (2008), *Final Report on Initial Database Design for a Database of CEUS Ground Motions*, Final Technical Report to the USGS for first year of Cooperative Agreement 07CRAG0015, 26 pp.

Cramer, C.H. (2016), Are potentially induced earthquakes different from natural earthquakes?, Seismological Society of America, 2016 Annual Meeting, April 20, 2016 (presentation and abstract available online at www.seismosoc.org under 2016 Annual Meeting Presentations).

Cramer, C.H., J. Kutliroff, and D. Dangkua (2009), *Second Year Final Report on a Database of CEUS Ground Motions*, Final Technical Report to the USGS for Cooperative Agreement 07CRAG0015-Mod1, 12 pp.

Cramer, C.H., J.R. Kutliroff, and D.T. Dangkua (2011), *Next Generation Attenuation East Initial Flat Files for Eastern North America*, Report to PEER accompanying NGA East flat files and time series under subagreement 7140, 4 pp.

Dreiling, J, M.P. Isken, W.D. Mooney, M.C. Chapman, and R.W. Godbee (2014), *NGA-East regionalization report: comparison of four crustal regions within central and eastern North America using waveform modeling and 5%-damped pseudo-spectral acceleration response*, Pacific Earthquake Engineering Research Center, Berkeley, California, PEER report 2014/15, October 2014.

Electric Power Research Institute (EPRI) (1993), *Guidelines for determining design basis ground motions*, Electric Power Research Institute, Palo Alto, California, TR-102293.

Erickson, D, D.E. McNamara, H.M. Benz (2004), Frequency-Dependent Q within the Continental United States, *Bull. Seis. Soc. Am.* **94**, 1630-1643.

Faddeeva, V.N. (1959), *Computational Methods of Linear Algebra*, translated by C.D. Benster, Dover Publications, New York, p 90-99.

Gallegos, A., N. Ranasinghe, J. Ni, and E. Sandvol (2014), Lg attenuation in the central and eastern United States as revealed by the EarthScope transportable array, *Earth Planetary Science Letters* **402**, 187-196.

Goldstein, P., D. Dodge, M. Firpo, Lee Minner (2003), SAC2000: Signal processing and analysis tools for seismologists and engineers, Invited contribution to *The IASPEI International Handbook of Earthquake and Engineering Seismology*, Edited by WHK Lee, H. Kanamori, P.C. Jennings, and C. Kisslinger, Academic Press, London.

Hough, S.E. (2014), Shaking from injection-induced earthquakes in the central and eastern United States, *Bull. Seis. Soc. Am.* **104**, 2619-2626.

Hough, S.E., and M. Page (2015), A century of induced earthquakes in Oklahoma?, *Bull. Seis. Soc. Am.* **105**, 2863-2870.

Joyner, W.B., and D.M. Boore (1993). Methods for regression analysis of strong motion data, *Bull. Seism. Soc. Am.* **83**, 469-487.

Joyner, W. B. and D. M. Boore (1994). Errata: Methods for regression analysis of strong-motion data, *Bull. Seism. Soc. Am.* 84.

McNamara, D.E., T.J. Owens, and W.R. Walter (1996), Propagation characteristics of Lg across the Tibetan Plateau, *Bull. Seis. Soc. Am.* **86**, 457-469.

Sedaghati, F., and S. Pezeshk (2016), Estimation of the coda-wave attenuation and geometrical spreading in the New Madrid seismic zone, *Bull. Seis. Soc. Am.* **106**, 1482-1498.

Silva, W., N. Gregor, and R. Darragh (2003), Development of regional hard rock attenuation relations for central and eastern North America, mid-continent and Gulf coast areas, Pacific Engineering and Analysis, El Cerrito, California, August, 13, 2003.

Thomas, W.A. (2010), Interactions between the southern Appalachian-Ouachita orogenic belt and basement faults in the orogenic footwall and foreland, Geological Society of America, Memoir 206, 897-916.

Toro, G., N. Abrahamson, and J. Schneider (1997), Model of strong ground motions from earthquakes in central and eastern North America: best estimates and uncertainties, *Seism. Res. Ltrrs.* **68**, 41-57.

Wessel, P. and W. H. F. Smith (1991). Free software helps map and display data, *EOS Trans. AGU* **72**, 441.

Zandieh, A., and S. Pezeshk (2010), Investigation of geometrical spreading and quality factor functions in the New Madrid Seismic Zone, *Bull. Seis. Soc. Am.* **100**, 2185-2195.

Publications from this Research

Publications are being prepared from this research but have not been submitted as of this date. Future papers based on this work will be provided, as required, when publication occurs.